University of Alberta

Effect of Heating Rate on the Thermal Properties of High Strength Mortar

by

Bingyu Xie

A thesis submitted to the Faculty of Graduate Studies and Research
in partial fulfillment of the requirements for the degree of

Master of Science
in
Structural Engineering

Department of Civil and Environmental Engineering

Fall 2019
Edmonton, Alberta

Abstract

Concrete is the most common building material in use in terms of per capita consumption. As demand increases continuously, the change in thermo-physical properties of concrete under sustained elevated temperatures has drawn attention. Although concrete is not combustible and possesses better fire resistance compared to other building materials, it is still limited when exposed to elevated temperatures. Explosive spalling for instance, is the most severe and critical mode of failure. The occurrence of explosive spalling in high strength concrete is especially of concern, due to the superior water tightness. The internal microstructure is further affected by the rate of heating, which in turn has a bearing on the thermal constants in higher strength mixtures. Therefore, the present study undertakes to examine how the thermal conductivity of cement-based materials is affected by different heating rates.

Two mortar mixtures, one designed for normal strength and the other, designed for high strength, were prepared for evaluatingthe role of heating rate on their thermal constants. Samples were extracted for test under three different heating rates ranging from 1°C/min to 10°C/min to a soaking temperature ranging from 200°C to 400°C. The thermal constants were measured using a hot disk thermal analyser system after approximately 30 min soaking at each target temperature. In order to understand the behavior of cementitious mortar under different heating rates, it is necessary to investigate the corresponding change in microstructural parameters and their impact on thermal properties. This study finds that the microstructure of high strength mortar is more sensitive to the heating rate compared to that of the normal strength mortar. Large cracks are observed in images at heating rates of 10°C/min for both mixtures, but images of high strength mortar show higher crack intensity. The porosity of both normal and high strength mortar increases with an increase in the temperature of exposure. However, the porosity drops for an increase in the heating rate. Additional image processing on back scattered electron images was made to evaluate the box count based fractal dimension. For both mixtures, the fractal dimension of the pores increases with an increase in the temperature. This study finds that the fractal dimension increases with heating rate. However,

this trend was more pronounced at lower temperatures of exposure, so that the fractal dimension becomes less conspicuous at higher temperature of soaking. The specific heat of mortar mixtures is mostly dependent on the presence of water at lower temperatures. However, the large cracks caused by thermal degradation may cause the specific heat of high strength mortar to decrease with an increase in the heating rate when exposed to temperatures beyond 300°C.

Acknowledgements

I would like to take this opportunity to express my grateful appreciation to my dear supervisor Dr. Vivek Bindiganavile for his technical advice, financial support and unconditional trust. I want to particularly convey my appreciation for his kindness and also this wonderful opportunity to pursue graduate study in structural engineering. Without his help, this research project would not be possible. I would like to extend my appreciation to Dr. Muhammad Mamun for his skilled assistance in Hot Disk measurements and image analysis. I am particularly grateful in his experienced support and suggestions in both manuscript and thesis writing.

This research study would not have been finished without technical support from staffs in several different laboratories at this university. I would like to especially thankful to Mr. Rizadly Mariano at the Civil Engineering Laboratory and to Mr. Greg Miller at the I.F. Morison Structural laboratory for their technical assistance in technical training and setting up different testing equipment and machines for this research. I sincere thanks to Mr. Mark Labbe and Mr. Walter Harley at the Thin Section Laboratory and Mr. Nathan Gerein at Scanning Electron Laboratory for their assistance in image acquisition. I am also grateful to the administrative staff of the Department of Civil and Environmental Engineering at University of Alberta for their assistance throughout the years and to the undergraduate summer student Mrs Hiba Al Shereida for their support and help.

Finally, I greatly appreciate my boyfriend Mr. Shaosen Ma and best friends namely Dr. Baolu sheng and Mrs. Huan ma in their suggestions and support for my research work. I am eternally grateful to my parents for their encouragement and guidance to this master program.

Table of Contents

List of Tables

List of Figures

Chapter 1 Introduction

1.1 Background

Concrete is a heterogeneous material composed of hydration products of cement and aggregates. It is now the most common building material and is second only to potable water as consumed per capita. With continuous growth of demand in building constructions, optimising the design of concrete member remains a top priority. Under extreme conditions like fire, the serviceability of concrete members can be seriously affected. Sustained exposure to high temperature changes the microstructure of the cementitious system, leading to a drop in the member capacity. Spalling is a common feature of fire damage, particularly in high strength systems. Since high strength concrete is more dense and impermeable than normal strength concrete, the damaging effect of fire and sustained high temperatures is likely to be more severe. It is seen that spalling of high strength concrete is in fact more violent and explosive that is often strong enough to cause secondary damage to adjacent members. As more high strength concrete is applied for members in high-rise buildings, the spalling of concrete members can be fatal.

As a result, understanding the behaviour of concrete at elevated temperatures has drawn attention throughout the 20th century. A review of investigation upon concrete spalling is presented first. Although the mechanism of spalling is still a mystery, studies report that internal stresses can be the main factors contributing to the phenomenon (Kodur 1998, Khoury 2005). The heating of concrete element involves mass transport into the pores. Water, both as a liquid and as steam inside concrete may be mobilized due to pressure gradient or molar concentration gradient (Mindeguia et al 2010). These fluids tend to move through the inner zone of concrete and start to condense into a moisture clog. The moisture clog can significantly increase pore pressures and initiate the spalling. Particularly in high strength concrete members, the low water to cement ratio causes the member to be relatively impermeable to fluid transport. Therefore, low water to cement ratio leads to even higher pore pressures, which then makes

high strength concrete vulnerable in elevated temperatures. Moreover, the material can be affected by the rate of heating, which is governed by multiple factors such as sources of fire, heating environment and distance to the source. The mass and heat transfer inside concrete is often dependent upon the rate of increase in the temperature. In this study, the experimental details and associated findings on the microstructure and thermal constants of mortar are made with two distinct mixtures exposed to elevated temperatures under different rates of heating.

1.2 Research Significance

The influence of heating rate when attaining a target high temperature, upon the thermal constants has not been investigated adequately for cement-based systems. The present study was undertaken to bridge this knowledge gap. In addition, using microscopy and image analysis techniques, the present study quantified the air-void network as it evolves under elevated temperatures and at various rates of heating. The air-void network is then correlated with the thermal constants.

1.3 Research objectives

This study aims to experimentally establish the influence of heating rate upon the microstructure of cement-based materials and relate that to their thermal constants. Specifically, the objectives are the following:

- To establish a relationship between thermal constants of cement-based mortar mixtures at sustained elevated temperatures and the rate of heating to reach that temperature;
- To quantify the microstructure at different heating rates using image analysis;
- To establish a correlation between the thermal constants and mortar micro-structure at different exposure temperatures using the concept of fractal geometry.

1.4 Organization

The investigation was focused on quantifying two key parameters namely, (i) thermal constants and (ii) the micro-structure. Both of them were obtained using an experimental approach. Whereas each of them is addressed in individual chapters, the two are later correlated to understand how high strength mortar behaves under various heating rates. The chapters in this thesis are organized as follows.

- Chapter 1 provides an introduction to this thesis. The background on spalling phenomenon and current research interest are described. And further, the research significance and objectives are presented;
- Chapter 2 provides the background information and review of previous work done on the spalling phenomenon. This is followed by a description of the state-of-the-art in regard to testing and characterization of thermal constants in cementitious systems;
- Chapter 3 describes the influence of heating rate upon the micro-structure of regular Portland cement mortar. Further tests were conducted by scanning electron microscopy with backscatter electron detectors followed by different image processing techniques to determine the porosity, pore size distribution and fractal dimension.
- Chapter 4 presents the experimental methodologies and findings on thermal constant measurements at different heating rates. Further discussion regarding the effect of heating rate on thermal constants is then provided. Eventually, the thermal properties are correlated with the micro-structure of the mortar mixtures that was quantified earlier;
- Chapter 5 enumerates the principal conclusions as derived from this study. In addition to their potential application, this Chapter also lists prospects for future works.

Chapter 2 Literature Review

2.1 Introduction

This chapter provides a brief review on those aspects of cementitious systems that are associated with thermal and physical change, when subjected to sustained elevated temperatures. Firstly, previous studies on the performance of different cement based systems under fire events are reviewed. As with other heterogeneous materials, the characteristic of each constituent namely, the hydrated cement paste and aggregates contributes to the thermal constants of the whole system. The behavior of the hydration products and the aggregates at different temperatures of exposure were essential to the study. Their chemical and physical behaviour were discussed with regard to effect upon the microstructure at different temperatures. In this study, the air-void network was quantified through fractal analysis, and so the fractal dimension of cement based systems and methods to evaluate the same are also reviewed.

2.2 Performance of concrete under fire and elevated temperatures

Prior studies reveal that normal strength concrete (NSC) possesses significant resistance to high temperature comparing to high performance concrete (HSC) (Kodur, 2013).

Concrete spalling is the most common phenomenon under fire. Studies (Ali 2001, Kodur 1998, Kodur and Phan 2007) have reported HSC being more sensitive to spalling phenomenon. Because of its lower permeability and higher stiffness, the resulting higher pore stress causes violent and explosive spalling in high strength concrete exposed to elevated temperatures. With an increase in the use of HSC, its performance under fire has come under greater scrutiny.

In modern building constructions, explosive spalling is considered as one of the biggest challenges for concrete fire safety design. On November 1996, the Channel Tunnel caught fire

that lasted for 9 hrs with the maximum temperature reaching an estimated 1000 °C (Lu 2015). The tunnel was made of high strength concrete with mature strength of 110 MPa. After the fire event, the 40 cm thick tunnel lining was foundhaving an average thickness of 17 cm after spalling. In the most severe section of the tunnel, the spalling depth have reached to 38 cm (Comeau 1997). The tunnel was reported severely damaged for 46 m, and the effected length was extended to 500 m (Kirkland 2002). The damaged section was repaired by 680 tons of plain shotcrete and 630 tons of fiber reinforced shotcrete (Liu 2015). Fire leads to the most dangerous form of concrete spalling, which can cause a sudden reduction of over 80% of concrete cross-section thickness (Liu 2015). This fact threatens the strength of the whole structural system, and can finally lead to a total collapse of the building. Kodur et al (2007) concludes that explosive spalling occurs during rapid heating and mostly in HSC, due to its low permeability. Explosive spalling occurs when the induced stress overcomes the tensile stress of concrete member, and local failure releases the built up energy, eventually leading to explosion of concrete members. However, there are studies (Bazant 1997, Muhammad 2018) that mention that pore stress alone cannot be the only factor that triggers explosive spalling. Since an increase in the temperature of exposure causes microstructural changes inside concrete, the pore stress will be mitigated after a certain point. Liu (2015) states that the combining effect of both thermal stress and pore stress is the main factor contributing to spall phenomenon. Khoury (2005) also reports that explosive spalling phenomenon happens in the early stage of the heating process. Moreover, HSC members when subject to lower heating rates exhibit a lower risk of explosive spalling (Ali et al, 2001). Kodur (1998) identifies six critical factors that directly influence the fire performance of concrete material:

- Compressive strength
- Concrete density
- Moisture content
- Specimen dimensions and shape
- Loading conditions
- Heating rate

The strength of concrete strongly influenced is performance under elevated temperature (Liu, 2015). Concrete members with higher strength are usually associated with lower permeability, which restricts its ability to allow evaporation during rapid heating. This may finally lead to explosive spalling. Kodur (2006) had also reported that replacement of Portland cement with silica fume could lower fire endurance, resulting instead in an increase in spalling. This was explained as due to a combination of higher water tightness and increased brittleness

The concrete density is closely related to its strength and water to cement ratio. A higher proportion of fine particles will both strengthen and densify a concrete mixture. This is accompanied with a reduction in the water to cement ratio. Now, concrete members with lower water to cement ratio tend to have much lower porosity than normal strength concrete. Therefore, high strength concrete is associated with lower permeability. As mentioned before, low permeability will reduce the ability of mass transfer during rapid heating. Mindeguia et al (2010) have found an inverse relationship of pore pressure and water to cement ratio, as shown in Figure 2.1 below. If pore pressure exceeds the strength of concrete, spalling may be triggered. However, Bilodeau et al (2004) found that lightweight aggregates can also increase the spalling because of its ability to absorb free moisture. They showed that of the moisture absorption by lightweight aggregate may lightweight concrete more susceptible. Clearly, of the moisture content of concrete plays an important role upon its fire safety.

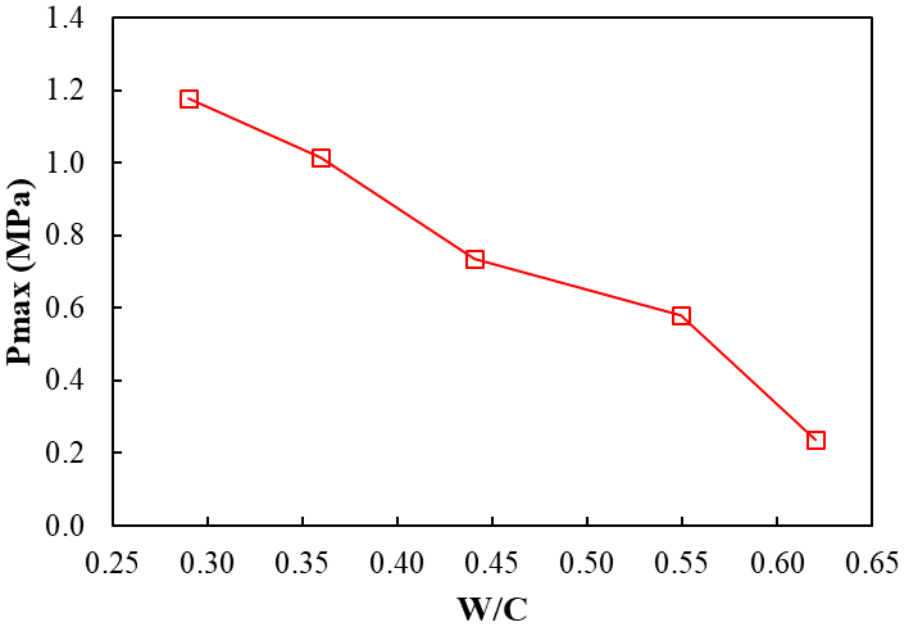

Figure 2.1 Maximum pore pressure as function of water to cement ratio (Mindeguia et al 2010)

The idea of linking concrete spalling to moisture content was not new. Earlier, Copier (1979) concluded that moisture content was an important factor affecting the spalling tendency. The results from many studies showed that concrete members with lower moisture content had less likelihood of spalling (Kodur 1998, 2003, 2007, Khoury et al, 2000). Meyer-Ottens (1972) found that the concrete with moisture content lest than 3.3% by weight did not spall, regardless of heating rate and applied stress. This could be thought of as a threshold as higher moisture content often led to spalling (Kodur, 2003)

The risk of spalling is also proportional to concrete member size (Kodur, 2007). This phenomenon may be explained by thermal gradients induced during fire events. Larger concrete members require a longer time duration for them to reach thermal equilibrium, and hence a thermal gradient is induced inside the member. Phan (2001) observed that spalling occurred at the time when the thermal gradient inside concrete specimens reached a maximum, showing that the induced strain energy from thermal stress was also significant in spalling mechanism. This thermal stress is accompanied with pore pressures. Thus, together it results in explosive spalling once the combined stresses overcame the maximum allowable concrete tensile stress. In addition to this, the thermal stress derived from the thermal gradient will

initiate micro-cracks, which then propagates as internal stress (Fu and Li 2010). Fu also pointed out that micro-cracks induced by thermal gradient was the key factor for corner and surface spalling.

Externally applied stresses are also a key factor that further reduced the fire resistance of a concrete members. While a number of researchers have reported that loaded concrete members were more susceptible to higher spalling (Kodur, 2006, 2007and 2013). The reason to this was that the externally applied stresses were added to internal stresses generated by thermal gradient and vapour. As a result, the concrete member became even more vulnerable when these stresses were superposed.

As mentioned above, rapid heating was one of the key factors to explosive spalling. The heating rate of concrete varies under different types of exposure and sources of fire (Hu et al 2011, Tran and White 1992). This is related to whether the fire is trigerred by hydrocarbons, or otherwise. For heating rates higher than 1°C/min, the occurrence of explosive spalling is more frequent in high strength concrete (HSC) than in normal strength concrete (NSC). Thermal gradients are induced during the rapid heating process on account of its relative low thermal conductivity and high specific heat. Fu and Li (2010) stated that heating rate was also associated with aggregate spalling, and surface spalling. The spalling phenomenon was seen to occur during the first 30 minutes of heating (Liu, 2015). When exposed to elevated temperatures, the building material may be affected by multiple factors. Figure 2.2 shows the temperature profile of gasoline and wood fires (Hu et al 2011; Tran H. C. and White H. R.). Comparing the three temperature profiles, one notes that the rate of heating is strongly affected by the distance from and the type of fire source. Therefore, fire safety of concrete should be optimised according to usage and surrounding environment conditions.

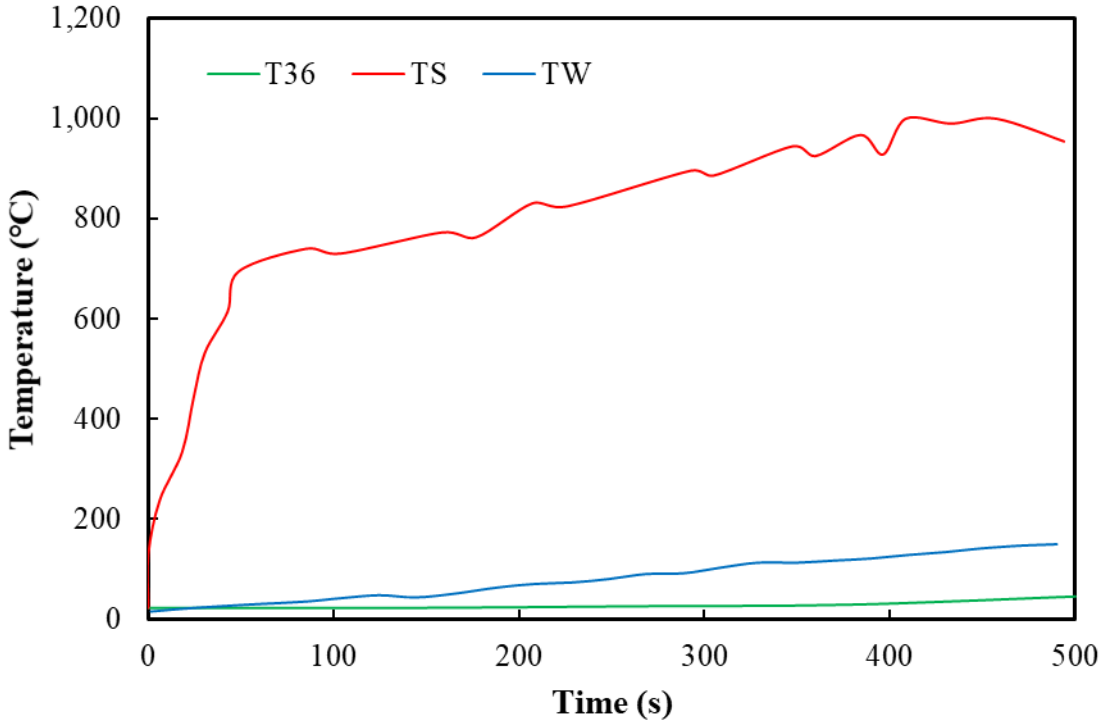

Figure 2.2 Temperature profile of gasoline and wood fires

Note: TW represents the temperature profile of rim walls holding gasoline pool fires. TS is the temperature of wood char surface and T36 is the temperature profile of a 36 mm char depth ((Hu et al 2011; Tran H. C. and White H. R.)

Aside of heating, Chan (2000) found out that the cooling regime affects the concrete compressive strength of HSC. In the case of specimen subjected to a peak temperature of 800°C, the drop in compressive strength for gradual cooling process was 4-6% higher than after rapid cooling. In addition, carbonate aggregate have higher specific heat than siliceous aggregates. Their use, coupled with that of polypropylene fibres is known to minimize risk of spalling in concrete members (Kodur et al, 2003a, 2003b, 2004, 2007). Chan (2000) further stated that the evaporation of polypropylene fibres in high temperatures would not lead to marked deterioration in strength.

2.3 Behaviour of Concrete at Different Temperatures

For heterogeneous materials like concrete, the macro mechanical properties play an important

role how it will behave at sustained elevated temperatures. Characterizing their behaviour through their constituent materials at different temperatures will help to understand and predict the system.

2.3.1 Behaviour of Constituent Materials

The constituent materials of a typical concrete include hydrated cement paste and aggregates. The products of hydration of the cement are up to 65 percent of calcium silicate hydrate (C-S-H), 20 percent of calcium hydroxide (CH) and about 15 percent of sulphoaluminate hydrates (Muhammad, 2018).

Upon heating, a concrete member loses water both physically and chemically. In the event of heating, free water in capillary pores starts to evaporate above 100 °C and chemical change occurs soon after due to loss of bound water. The water chemically bonded in C-S-H vaporizes at a temperature range of 100 - 300°C, and the peak rate of loss occurs at approximately 270°C (Al-Sibahy and Edwards 2012, Formosa et al 2011). Thereafter, the calcium hydroxide crystals decompose into calcium oxide and water vapour near 400°C (Shoaib et al 2001) as follows:

$$Ca(OH)_2 \rightarrow CaO + H_2O \qquad (2.1)$$

The resulting calcium oxide can be rehydrated to calcium dioxide if the concrete member are exposed to high moisture environment after heating (Shoaib et al 2001). However the rehydration process is usually accompanied with expansion, causing further damage to the concrete member. Formosa et al (2011) has confirmed the further decomposition of C-S-H takes place at temperature beyond 600°C based on SEM investigations. The hydrated phases including C-S-H and CH are amorphous near 1150 °C and not crystalline unlike under room temperature. (Sibahy and Edwards 2012)

In addition to C-S-H gel and portlandite, decomposition of calcium aluminates also take place as temperature rises. Ettringite ($Ca_6Al_2(SO_4)_3(OH)_{12}\cdot 32H2O$) is considered thermally unstable when temperature reaches ~100 to 125°C. The compound partially loses water molecules as the temperature rises, and eventually it decomposes into $C_4A_3\overline{S}$, $CaSO_4$ and CaO (Zhou and

Glasser 2011).

2.3.2 Weight Loss

Weight loss results from moisture evaporation, and is a measure of concrete deterioration during heating. As mentioned earlier in the previous section, C-S-H starts to vaporize once the temperature reaches approximately 100°C. The loss of chemically bound water is critical to the fundamental fracture properties (strength, brittleness and etc.) of concrete members. Ye et al (2005) has monitored the weight loss of traditional, self-compacting and high performance concrete with temperature up to 1200°C. The weight loss in Figure 2.3 represents the decomposition of C-S-H, CH and calcium aluminates from 105 to 450°C (Sibahy and Edwards 2012, Ye et al 2007, Zhang 2011, Zhou and Glasser 2011). The investigation was on a concrete mixture with compressive strength of 67 MPa at room temperature. Besides the effect of temperature, results in Figure 2.3 also show higher weight loss with longer exposure time. However, all curves reach a plateau with sufficiently long exposure time, which indicate the hygric equilibrium state of concrete. A hygric equilibrium state can be reached at certain time of exposure, but longer exposure time is required for lower heating temperatures (Zhang 2009). In addition, there are many factors influencing the rate of weight loss in high temperatures. Results from Sancak (2008) indicate that concrete containing higher amount of silica fume exhibits high weight loss.

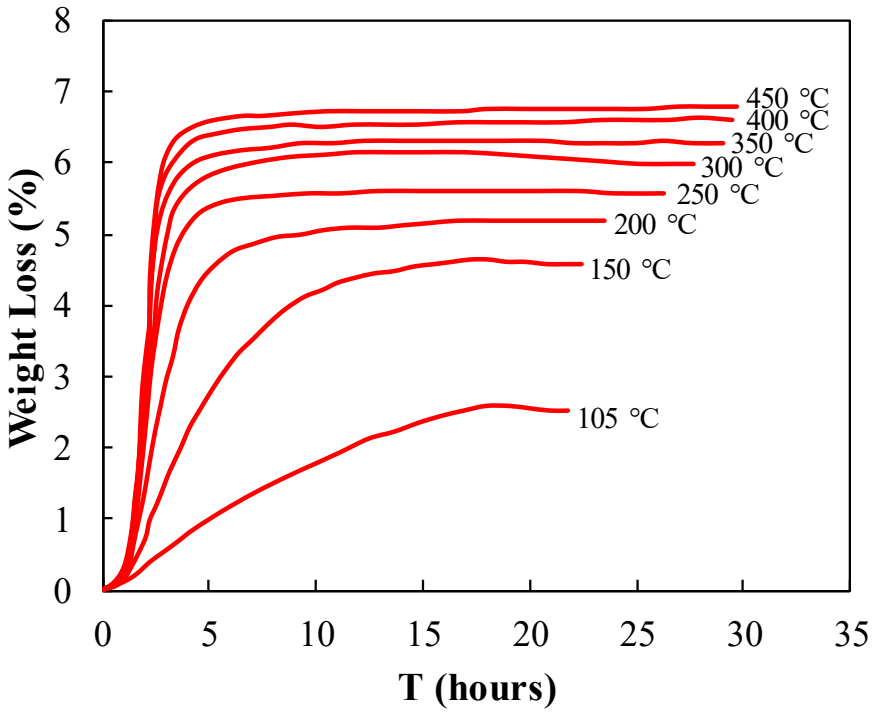

Figure 2.3 Weight loss over the complete heating process for different heating temperatures (Zhang 2011)

2.5 Microstructure

As mentioned in the previous section, the products of hydration are sensitive to temperature change. At elevated temperatures, both crystalline and non-crystalline products undergo physical change that alters the microstructure inside concrete material. This change can have a significant effect on thermal and mechanical properties of a concrete member. In this section, a brief review of temperature variation as affecting the micro-structure is presented.

2.5.1 Porosity

The porosity and pore structure are important to a concrete member as they are rate controlling factors for harmful chemical agents, such as chloride ions, acids and carbon dioxide (Della 1988). In the meantime, porosity also has a close relationship with concrete mechanical and thermal properties. The porosity of concrete increases with temperature, which is the major effect of decomposition of hydration products.

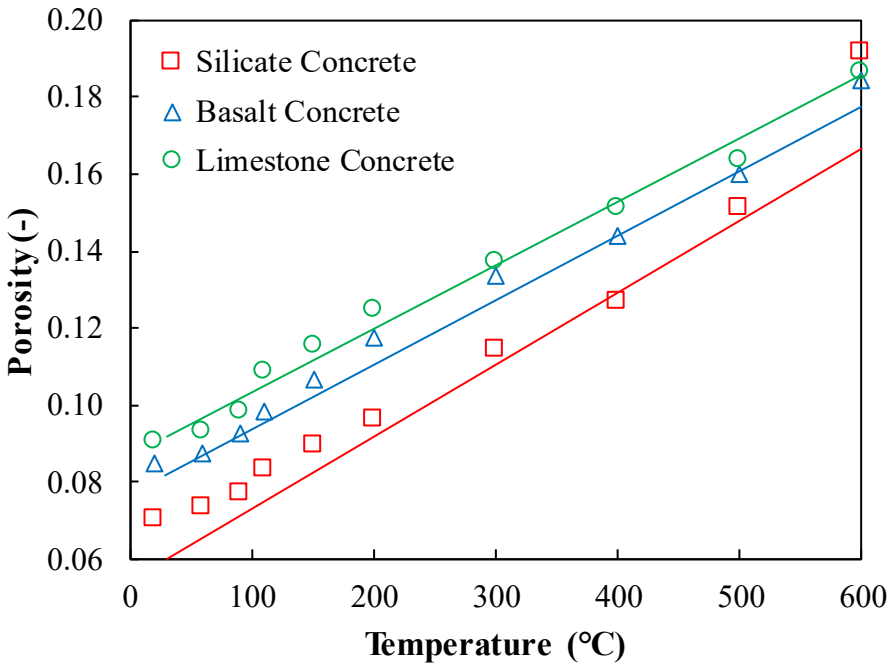

Figure 2.4 Total Porosities of different types of concrete with the increase in temperature (Gawin et al 1999)

The porosity percentage increases nonlinearly with respect to temperature. Rostasy et al (1980) reports that the total volume change of pores is relatively small below 300°C, then a significant increase of porosity happens when temperature rises beyond 600°C. Gawin et al (1999) is able to compute an approximate linear relationship through experimental values with the maximum temperature of 600°C. Figure 2.4 above shows that all three types of concrete investigated clearly follow the similar pattern up to this point. In early this century, Vodák (2004) has conducted an experimentation on porosities of the unsealed concrete samples at varies of temperatures. The role of elevated temperature on porosity change is revealed up to 900 °C, as in Figure 2.5 below. Similar as Rostasy has reported in his work on concrete porosity, the data shows much smaller relative growth of total pore volume below 450°C. In addition to this, the further characterization in total pore volume change beyond 600°C is also confirmed. As one can see, the total pore volume starts to increase nonlinearly at higher temperatures, and a significant jump is observed at 800°C.

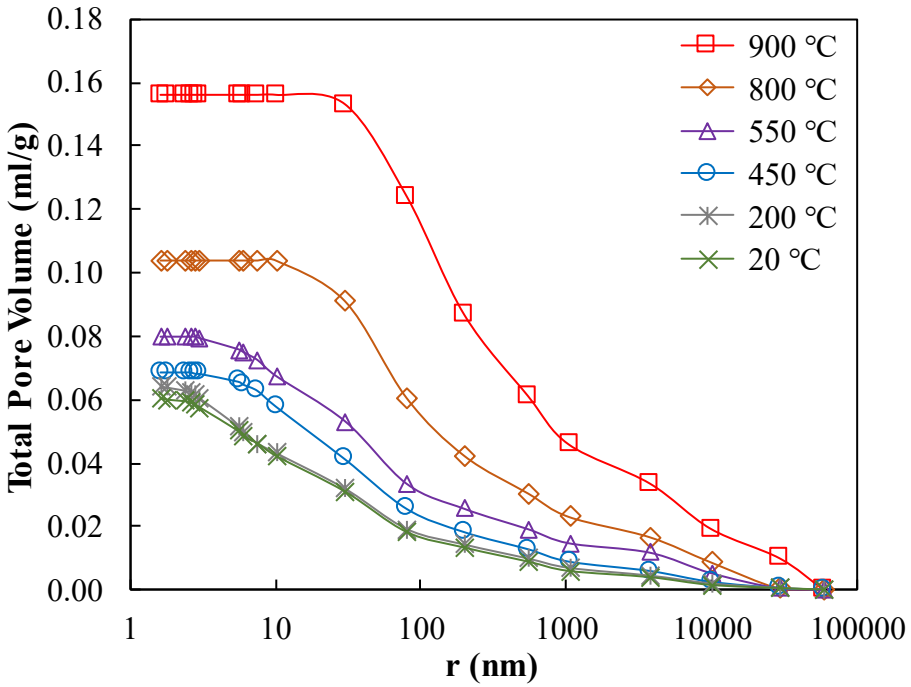

Figure 2.5 Effect of total volume of pores on pores sizes at different temperatures (Vodák et al 2004)

Porosity of concrete is also associated with its permeability, which can be defined as the ability and quality for materials to transmit a fluid (Charlaix et al 1987, Pierre K 2001). The permeability of a porous media is controlled by the smallest path of interconnected pores. Pierre (2001) have mentioned that the interfacial transition zones (ITZ) of concrete contribute the weakest link of the pore system regarding permeability. Therefore, ITZ of concrete can be significant to its permeability

ITZ is the region in the vicinity of the aggregate particles, where the microstructure of the coment past is modified (Ollivier 1995). It is the most important interface in concrete. During casting of concrete, the porosity and water to cement ratio increase toward to the surface of aggregate. Consequently, the excessive water content causes micro-bleeding and accumulation of water under the aggregates before setting. Snyder (1991) claimed that a continuous easy path can be established across ITZ, causing high permeability and rapid diffusion of dissolved particles. Moreover, Diamond (2001) observed approximately up to 30% increase in porosity surrounding an aggregate from examinations of SEM specimens. In addition, additional

content of CH and Aft phase were found within the ITZ than in the bulk cement paste (Grandet 1975). Note that the crystalline products do not provide strength to the concrete material. As a result, ITZ is often the weakest spot inside a concrete material. Upon extremely exposure, thermal induced cracks tend to propagate through the weakest zone (Muhammad 2018). Therefore, large cracks can often be observed surrounding an aggregate. The cracks within the ITZ further prevent heat transfer between the cement paste and aggregates, resulting in high thermal gradient inside a concrete material. Pierre (2001) stated that HSC had very thin ITZs. This observation can be one of the reason such that HSC is much sensitive to explosive spalling at high temperatures.

2.5.2 Pore size distribution

There are many ways to determine pore size distribution in concrete. Among the techniques, mercury intrusion porosimetry (MIP) and image analysis are well-known, and have been conducted by many studies in exploration of pore systems. MIP technique provides valid estimation of total porosity, pore volumes and pore size distribution of a porous solid. However, limitations exist in this method to truly reveal the actual pore size distribution of cement based materials. Nowadays MIP technique is only valuable to provide feature of pore structure, such as threshold diameter and connectivity (Diamond 2000). The image analysis, on the other hand, is able to provide better estimation of pore fraction and sizes through backscatter SEM views, using pixel counting and morphological opening operations.

Many studies have observed coarsening effect of pore structure under elevated temperatures (Chan et al 1999, 2000a, 2000b, Della 1988, Diamond 1999, 2000, Xu et al 2001, Ye et al 2007). The pore coarsening effect can be attributed to evaporation and thermal decomposition hydration products of cement paste. Chan et al (1999) indicated that both normal and high strength concrete experienced coarsening effect on microstructure. Both types of concrete showed almost the same degree of damage, but HSC suffered more to the permeability related durability. Similarly, Xu et al (2001) found out an significant increase of pore diameter of pulverized fly ash concrete after exposure to 250°C. However, the coarsening effect mainly

occurred at a higher temperature of 450°C. Moreover, Ye (2007) conducted a detailed investigation on concrete samples at different depth from the exposure surface. It had no doubt that the pore volume and critical pore diameter increase toward to the heating surface. In addition to his study, the presence of polypropylene fibres was found to have positive influence to the damage of microstructure at high temperatures. The melted polypropylene fibres increased connectivity of pore system, so that water vapor could escape from the inside without causing further damage.

2.5.3 Fractal Dimension

Mathematically, a fractal dimension provides a complexity index which can be expressed as the scaling of an object's bulk with its size. (Theiler 1990). The concept of fractal geometry was initially developed by Mandelbrot (1982), which he derived mostly from the work done by Richardson (1961). The concept was originally used to study cartographic boundaries on map surfaces. Richardson found out that the measured length of land-sea boundary on the geometrically irregular west coast of Britain changes with the length of the measuring stick used. Measurement with smaller stick always produced longer coast length. After trials of repeated measurements with different sizes of measuring stick, he concluded a linear relationship of the logarithm of the total boundary length against the logarithm of the stick length, with a negative slope (Diamond 1999). The slope was then defined as the fractal dimension, which was usually cast as an equation of the form (Theiler 1990):

$$D_f = \lim_{size \to \infty} \frac{\log area}{\log size} \qquad (2.2)$$

Where D_f is the fractal dimension.

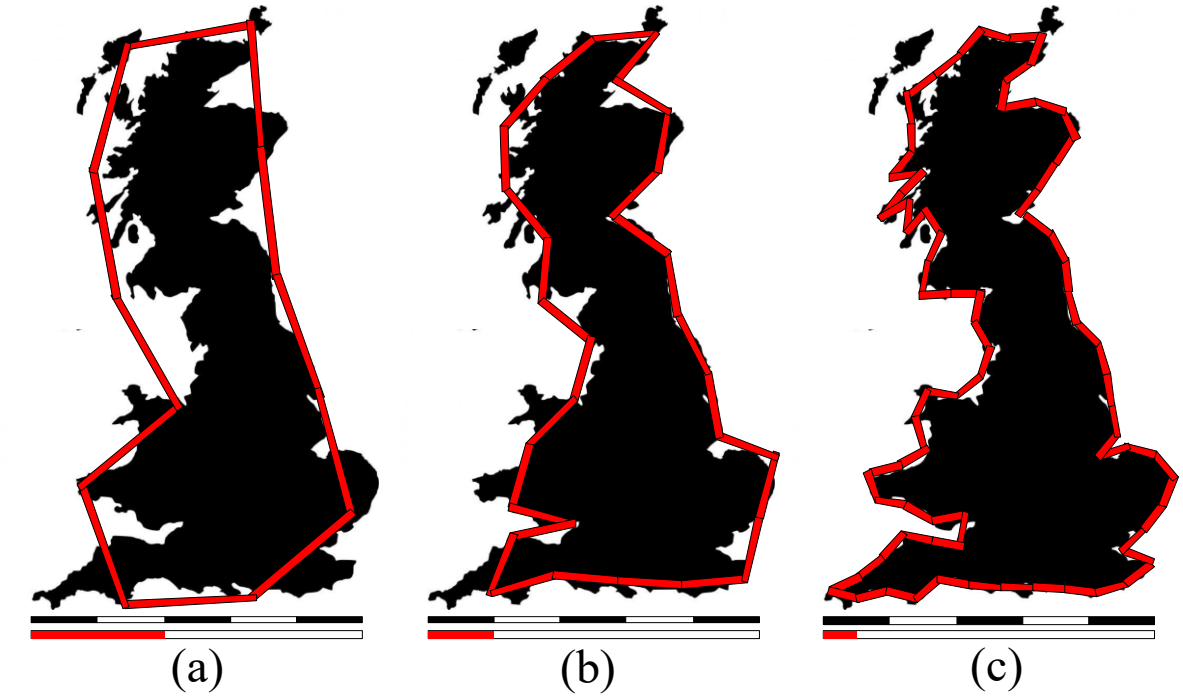

Figure 2.6 Measurement of cartographic boundaries using different length of stick. (a) to (c) shows the measurement of British coastline with decreasing scale for the measuring stick. As the scale of the stick decreases, the measured detail and total length of coastline increase.

If the rate of increase in observed object area against a decreasing measuring scale length remains constant at any degree of magnification, then the object can be described as self-similar. Self-similarity is the hallmark of a fractal surface (Diamond 1999). Russ (1992) categorizes fractal surface into three classes. Among them, dense objects having a distribution of holes or pores with a fractal structures, can be defined as pore fractals. As a result, porous solid as concrete can be described using fractal geometry.

There are many techniques available in determining fractal dimension of a concrete surface (Diamond 1999, Wang 1995, Wang and Diamond 2001). With the power measurement technique employed in studies of concrete, several discoveries of pore features have been found. Winslow (1985) used an X-ray scattering technique for measuring the fractal dimension of a cement paste surface. Upon examination, cement paste with highly irregular surfaces with fractal in character were confirmed. In addition, the water to cement ratio variation provided some influence on the irregularity with lower ratios producing rougher surfaces (Winslow

1985). Wang (1995) conducted fractal analysis on cement paste using box-counting method from back scattered electron (BSE) images. He observed pore feature on the sample surfaces exhibit two fractal regimes under different resolution of images. Based on Wang's observation, images at low resolutions showed a structural fractal dimension isranging from 1.05 to 1.15, where a textural fractal dimension was presented under higher resolution is ranging from 1.22 to 1.49.

2.4 Thermal Constants

The thermal constants are key parameters that governs the heat resistance of concrete materials in fire conditions. Thermal conductivity and specific heat or specific capacity are two important thermal constants, which have drawn many attentions in concrete fire safety researches since last century. These two thermal properties effect the temperature rise as well as the thermal gradient inside a concrete member (Kodur 2003). They are essential in developing models and predicting the temperature distribution in heated concrete. These information together provides better reveal of thermal characteristics of concrete, and further helps in prediction of its thermal behaviour.

Thermal conductivity and specific heat can be measured using varies of techniques. The most commonly used measurement techniques can be divided into steady-state and transient methods. In steady-state methods, the thermal properties are measured with a constant temperature difference with respect to time. In transient methods, the measurements require detection of temperature dissipation in a short period of time (usually in seconds), and a temperature change profile with time will also be developed.

In this study, transient plane source (TPS) method is used to measure both thermal conductivity and specific heat. Transient plane source, also known as hot disk method, uses a plane sensor as both a heat source and a temperature sensor. TPS method requires testing samples to be sliced into halves, and the hot disk sensor is sandwiched in between. During the measurements,

the sensor surface heats up a little, and this temperature dissipation over a short period of time is monitored. The temperature change verses time will then be plotted, and both thermal conductivity and specific heat can be described with application of a mathematical model (Bouguerra et al 2001). This method is capable to cover a thermal conductivity range of 0.01 to 500 W/m/K for both isotropic and anisotropic materials. The testing standard and procedures are specified in ASTM D7984 and ISO 22007-2.

2.4.1 Thermal conductivity

The thermal conductivity is a measure of a material's capability to conduct heat when it is subjected to a temperature gradient. In another word, thermal conductivity plays a dominant role on the rate of heat transfer inside a material as well as its performance in high temperatures. The thermal conductivity can be defined as:

$$\kappa = \vec{Q} \cdot \frac{dt}{dT} \qquad (2.3)$$

Where κ is the thermal conductivity, $\vec{Q}$ is the heat flow rate or heat flux. It is a vector in the direction of a cross sectional area perpendicular to heat flow rate $\vec{Q}$ and the absolute temperature T, and t is the time (Yang 2004).

The thermal conductivity of a concrete material mostly rely on its constituent materials, ambient temperature as well as moisture content (Muhammad 2018). Similarly, Kim et al (2003) investigated seven parameters which showed marked influence on thermal conductivity of concrete: early age, coarse and fine aggregate fractions, amount of cement, and types of admixtures, temperature and moisture content. Note that the age of concrete only gave effect on thermal conductivity in very early ages (about 2 days), but the age could barely influence the measured thermal conductivity once the concrete age became older enough (Kim et al 2003).

The thermal conductivity of concrete decrease as temperature increases. The decrease of thermal conductivity above 100°C is associated to the decomposition of calcium aluminates (Aft phases). The water chemically bonded in calcium silicate hydrate (C-S-H) also evaporates

at this point, the porosity increases and so as the propagation of micro-cracks. The combination of these phenomena become a very effective heat transfer barrier, therefore a marked decreasing trend in thermal conductivity from 100 to 400°C has been revealed in many experimental investigations (Santos 2003). Thus, the thermal conductivity has opposite correlation with concrete porosity level. Santos (2003) was able to establish a linear relationship of thermal conductivity against porosity level. The thermal conductivity decreases as the porosity level increases no matter the temperature either rises or drops. In Figure 2.7 below, concrete samples are first fired for 6 hrs at 1000°C and then cooled to room temperature before re-heating, where A1 to fds indicate concrete samples with increasing porosity. The measurements are carried out using the fired samples in 100°C intervals till the exposure temperature of 1000°C. The results reveal a smooth decreasing trend of thermal conductivity as porosity level increases, which the change in thermal conductivity remains relatively constant over temperature.

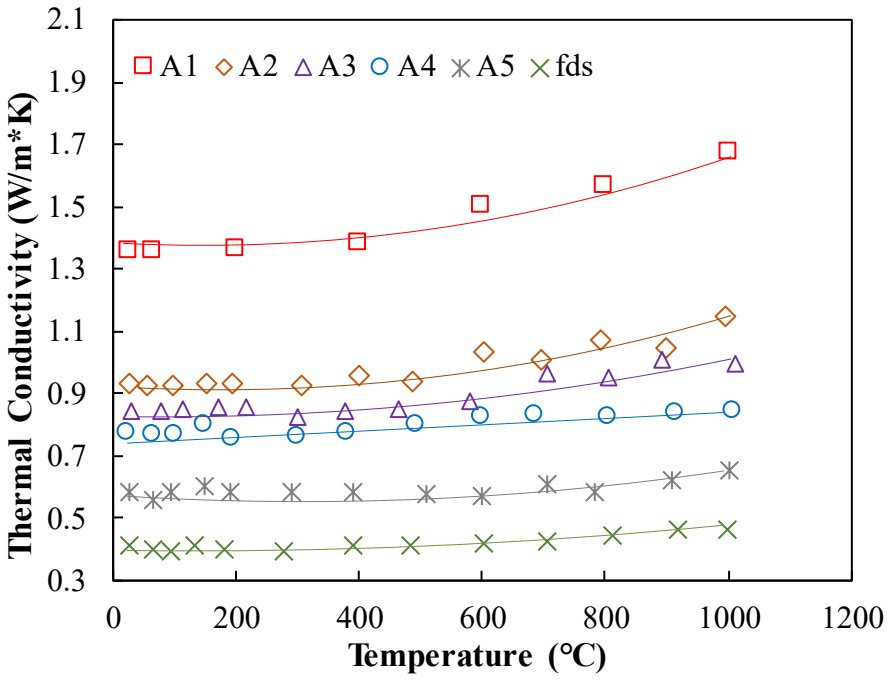

Figure 2.7 Thermal conductivity as a function of temperature for already heated concrete sample (Santos 2003)

The aggregate type affects the thermal conductivity of concrete significantly (Khan 2001).

Calcareous aggregates such as limestone are less conducting than siliceous aggregate. The latter is more crystalline promotes the heat flux (Muhammad 2018). The higher the crystallinity of aggregates, the higher the measured thermal conductivity. The crystallinity of concrete constituents will influence their thermal conductivity at high temperatures. Kodur (2013c) experimentally investigated two plain high strength concrete (HSC) with carbonate and siliceous aggregate types respectively. It is seen that siliceous aggregates show higher thermal conductivity than calcareous aggregate in the temperature range over 200 whereas they both have similar thermal conductivity below 200°C.

2.4.2 Specific Heat

The specific heat or heat capacity is the amount of energy per unit mass required to change the temperature of a material by one unit. It can be expressed as

$$c = \frac{1}{M} . \frac{dQ}{dT} \tag{2.4}$$

Where M is the mass of the sample, dQ is the amount of heat needed to raise a small increment of temperature dT on the sample.

The specific heat of concrete can be effected by its moisture content, type of aggregates and density (Kodur 2003c, 2014b). Like thermal conductivity, specific heat of concrete is sensitive to both physical and chemical mass transfer in elevated temperatures. The physical mass transformation is mostly caused by dehydration of solids phase in lower temperatures, such as the vaporization of free water at 100°C. Since the specific heat of water is much greater than the solid phase of concrete, the overall specific heat of concrete initially increases with temperature raise until the concrete starts to dry out. Therefore, the specific heat of concrete as a function of temperature exhibits a peak at 150 to 200°C (Kodur 2003c, Santos 2003). Furthermore, Kodur (2003c) observed another peak above 400°C for HSC, which was mainly caused by removal of crystallized water bonded in the cement paste.

As with thermal conductivity, the specific heat of concrete at higher temperatures is also sensitive to the aggregate type. Here too, the specific heat for high strength concrete with carbonate aggregates was generally higher than the sample with siliceous aggregate (Kodur, 2003c). This may be attributed to the lower thermal conductivity of carbonate aggregate. As the result, more thermal energy was required to produce the same temperature rise in carbonate aggregates compare with that for siliceous aggregates. This difference in specific heat is found to become more significant above 600°C. Kodur (2003c) observed a big jump in the specific heat for dolomitic aggregates at this temperature, which was likely caused by their dissociation into calcium and magnesium carbonates.

Chapter 3 Image Analysis on Microstructure of Normal and High Strength Mortars at High Temperatures under Different Heating Rates

3.1 Introduction

Mortars as the specific form of concrete, are heterogeneous materials containing mainly the hydration products and fine aggregates. C-S-H phase occupies up to 65% of cement paste hydration products, and has the most contribution of strength to the concrete materials. In HSC, application of silica fume provides additional source of silicates, which further bind with CH to produce more C-S-H phase. As a result, the HSC can achieve much higher compressive strength compared to NSC. The C-S-H phase has non-crystalline structure with high specific surface area (Muhammad, 2018). The water chemically bonded in C-S-H phase begins to evaporate at 100°C. Enlarged voids resulting from water evaporation then increase the total porosity inside mortar. Studies have found a conspicuous weight loss associated with dehydration of C-S-H within a temperature range from 100 to 400°C (Chan 1999 and Noumowe 2005). Hydration products with crystalline structures such as CH and calcium aluminates or ettringite contributes to the rest of the hydration products volume. The crystalline hydration products do not contribute to the strength of concrete, but play an important role in their thermal properties. In the interfacial transition zone (ITZ), the concentration of crystalline materials like CH and ettringite is considerably higher than deeper into the hydrated paste (Diamond and Huang 2001). For this reason, the ITZ around aggregates usually have limited strength. In addition, the ITZ also contains extra porosity which further weakens the area. In HSC, the presence of silica fume fills up the extra porosity inside ITZ due to its finer particle size, so that the ITZ is almost eliminated (Diamond and Huang 2001). However, when the temperature rises at a certain rate, the impact to ITZ is significant, as cracks develop surrounding an aggregate. As mentioned earlier in previous chapters, the thermal decomposition of ettringite starts around 100°C. As the temperature increases, the ettringite gradually loses water molecules until it eventually decomposes into $C_4A_3\overline{S}$, $CaSO_4$ and CaO (Zhou and Glasser 2011). In the meantime, both pore pressure and porosity inside the ITZ

increase, and finally cause large cracks around aggregates. This phenomenon does not only effect the strength of concrete, it also produces significant impact on thermal properties. The cracks formed inside ITZ act as barriers to prevent transmission of heat. Thus, thermal conductivity of concrete member tends to drop at high temperatures, which further aggravates the thermal gradient inside the concrete. For HSC, thermal gradient and induced pressure are the main factors to explosive spalling.

The mass transfer of both crystalline and non-crystalline phases in high temperatures will result in the change of total porosity. Since variation of porosity is considered as one of the main effect on thermal properties of concrete, it is necessary to take a close investigation on the relationship of heating rate and porosity change. In the meanwhile, the pore size distribution of concrete also changes as temperature increase. Luo et al (2000) investigated variation of porosity under exposure to high temperature for both NSC and HSC. The change in porosity of HSC was found significantly higher than NSC, but the total porosity of HSC was still lower than NSC. The pore size distribution of HSC showed a marked increase for all radii at the same time, known as the pore coarsening effect (Chan et al 2000 and Luo et al 1999). All these studies together have drawn a map that describes the relationship between temperature and micro-structure of concrete in great detail. Yet, they still miss the relationship between concrete micro-structure and heating rate. This relationship will eventually address how the thermal constants change at different heating rates.

The studies mentioned above involved mercury intrusion porosimetry (MIP) in their research on concrete micro-structure. However, limitation existed in conducting MIP to explore the nature of pores in hydrated cement systems. Diamond (2000) indicated the failure of the MIP method on identifying pore size distribution from hydrated cement systems. The failure was intrinsic and was mainly caused by the two assumptions in the Washburn model: (1) the pores are cylindrical and (2) the pores have equal accessibility to the outer surface of the specimen. It is obviously that the pores in concrete specimens were not all cylindrical. The first assumption clearly exposed the limitation of MIP method on the accuracy of modelling the

nature of pores. The second assumption lead to misallocation of larger pores to the diameter of the smaller pores. This failure of calculation resulted the calculated pore size distribution was always smaller than the actual pore size distribution of the specimen. Although MIP method could be useful in providing threshold pore sizes and pore space measurements, accuracy still remained as a big challenge to explore the true nature of concrete micro-structure (Diamond 2000). As an alternative way to solve the problem, image analysis of backscattered electron images was introduced to later studies in concrete researches (Diamond 2000, Diamond and Huang 2001, Wang and Diamond 1994, Wong et al 2006). It is worth mentioning here that the main limitation of this technique is spatial resolution (Scrivener 2004). Since the images are taken from two dimensional sections of a three dimensional object, the actual features of the structure may not be fully revealed. The most common problem of using this technique is that the section does not always pass equatorially through a pore, therefore the actual pore size can be underestimated. Moreover, pores appearing unconnected in a two dimensional image may actually be connected in three dimension.

3.2 Objectives

The dehydration of ettringite and C-S-H phase has significant influence on the microstructure of concrete as temperature increases up to 400°C. The microstructure then has close relationship to the thermal properties of concrete. As mentioned earlier, investigation on micro-structure change with different heating rates is still missing in current studies on concrete properties at high temperatures. Therefore in this chapter, the image analysis using scanning electron microscopy (SEM) with backscattered (BSE) detector is introduced to explore the nature of concrete microstructure at different heating rates. First, the change in total porosity at different heating rates and target temperatures is discussed. Then, the pore size distribution at different heating rates measured from backscattered electron images are presented. Finally, the nature of mortar microstructure is evaluated by fractal dimension. In addition, the measured pore data is studied and compared with weight loss and thermal constants in the next chapter.

3.3 Experimental Procedure

3.3.1 Mix Design

The mixture proportions of normal strength mortar (NSM) and high strength mortar (HSM) prepared for this study were listed in Table 3.1. In addition, a high range water reducing admixture (HRWRA) was added to NSM and HSM mixes, at 1.5% and 1.2% by weight of cement, respectively, to improve the flow of fresh mortar. HRWRA was also known as superplasticizer, which can reduce water content by 12 to 30% to maintain workability. The dosages of HRWRA for both mixes were determined by trials until suitable flow rates (less than 200%) are achieved from standard flow table test (ASTM C1437). The final water to binder ratio for two mixes are 0.5 and 0.35 respectively.

The composition of aggregates plays an important role in concrete behaviour under elevated temperatures. Therefore the use of fine aggregates is restricted to a single source of manufactured silica sand to eliminate any potential variation factor. The silica sand is blended from three types of gradations, so the particle size distributions of fine aggregates used in both mixtures are kept identical in the same purpose throughout the study. The particle size distribution of silica sand are sieved under the procedure specified in ASTM C33, and the plot detail can be found in Figure 3.1 below. Note that a much higher proportion of silica sand by weight of cement is used in NSM compared with HSM, which had only 60% by weight of cement being used in the mix.

Cement used in the mix meets the requirements of CSA C3001 for type GU, and fly ash is classified as Class CI under CSA A3000. 15% of silica fume by weight of cement was added to the HSM mixing to achieve higher strength. Note that class C fly ash and silica fume contains relatively finer particles than type GU cement, both materials provide additional source of calcium and silicate. With enough time and source of water, additional C-S-H can be produced from further hydration process. Although this additional C-S-H contributes more strength for HSM, it can behave very differently in high temperatures because of evaporation of crystallized water. Moreover, high proportion of cement with the use of fly ash and silica fume has resulted

relatively higher density of HSM, which can be found in Table 3.2.

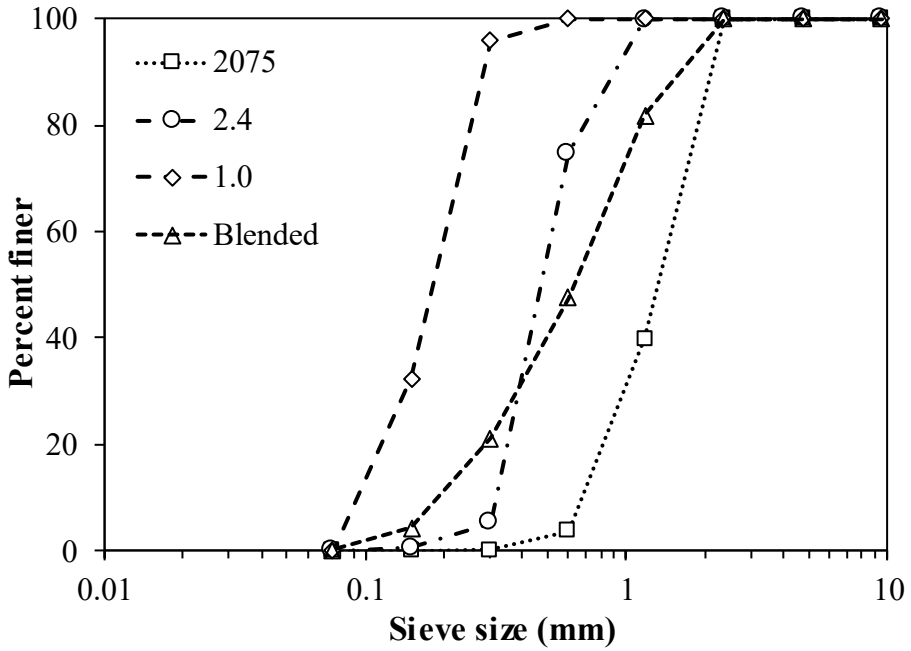

Figure 3.1. Particle size distribution of silica sand mixed in NSM and HSM samples

About 0.2% of polyester fibre (PET fibre) is added by volume in both NSM and HSM mixture in order to prevent potential hazard of explosive spalling. This fibre is a well-known synthetic fiber derived varies of sources, such as petroleum and recycled bottles. Application of PET fibre in mortar helps in preventing early cracks, and also improves mechanical performance by increasing flexural and impact toughness (Fernando 2012). PET fibre has melting temperature of approximately 250°C (Silva 2004). The melting of PET fibres beyond 250°C will have an influence on thermal constants due to further increase in the total pore volume.

Table 3.1. Mixing proportions (kg/m^3)

	NSM	HSM
Cement	428	728
Water	214	255
Silica sand	1286	437
Silica fume	0	109
Fly ash Class C	0	109
HRWRA	6	8.7
PET fibre	1.81	1.81

Table 3.2. Sample Properties

	NSM	HSM
Dry Density (kg/m3)	2023	2132
Flow table test (%)	175	170
7 day compressive strength (MPa)	20.4	83.19

In order to achieve consistency of measurements from both image analysis and thermal test, the mortar specimens used in SEM with backscatter image exam were prepared with the same mix design and procedure as the specimens used during the thermal test.

3.3.2 Specimen Preparation

The mixture of NSM and HSM was prepared using a rotary high speed mixing machine. During mixing, dry materials with desired amount of water were mixed under high speed of 30 cycle/s for 10 minutes. Afterwards, PET fibre was gradually added to the mixer and another 10 minutes of mixing was applied to allow proper disperse of fibre.

The fresh mortar was contained into 50 X 50 X 225 mm prism followed by 5 minutes of mechanical vibration for proper compaction based on ASTM C192/C192M—16a. After cast, mortar prisms were kept in humidity room with relative humidity of 95% and controlled temperature of 23°C. Accelerated hydraulic curing was applied at mortar age of approximately

24h, following procedure ASTM STP 169 D. Note that in the original procedure, the specimens were kept in molds and immersed in boiling water. Because of the limited size of water tank, the temperature was set at 95°C to avid boiling. In addition, specimens were de-molded since plastic mold might melt and damage the tank. After 3.5 h of hydraulic cure in water bath, mortar specimens were stored back to humidity room until the same day of thermal test. The specimens for image analysis were cut into 10 X 10 X 10 mm cubic dimension before heating. Then, they were positioned beside thermal test specimens for each test with 1 °C/min, 5 °C/min and 10°C/min heating rate respectively. Note that all thermal test and image analysis specimens are pre-dried in oven at 100°C with duration of approximately 24h. Therefore, the cubic specimens experienced the same heating condition as the mortar specimens for thermal test. Afterwards, the sample cubes were prepared for SEM with BSE detector imaging using hardened epoxy resin. The blue dye epoxy resin with low viscosity was impregnated into the specimens under vacuum condition, then cured for 24h at room temperature. The reason to involve epoxy resin in image analysis of hydrated cement system was mainly because of its low backscatter coefficient. Since the viscosity of epoxy resin was low enough to fill surface pores on mortar specimens, the pores would appear dark in SEM image. Impregnation of epoxy resin also prevents potential damage during polishing process and shrinkage cracking. After curing, the extra part of harden epoxy resin was grinded off to the sample surface. The exposed surface was then polished mechanically using finer polishers with diameters of less than 1 μm.

3.3.3 Image Analysis

The SEM images are captured using Zeiss Sigma 300 VP-FESEM equipped with backscattered electron detectors. Each image is acquired at an accelerating voltage of 25kV and resolution of 1024 X 768 pixels. The captured images require further quantification of image features to obtain accurate and consistent data. The image before quantification process contains different brightness intensities, or grey levels. Note that this type of images contains 8-bit grayscale with intensity value from 0-255 (Muhammad 2018). In order to acquire pore features, the 2D greyscale images must be transformed into binary images by establishing grey level threshold. The obtained binary images will only have intensity scale from 0-1. There are several ways to

find threshold of grey intensity to distinguish pores from solid. The method in Wong (2006)'s study is adopted to find a critical point where the established threshold value would create a binary image precisely revealing the pore features. In this study, pixels of captured images were divided into 63 segments with increasing of grey levels. As shown in Figure 3.2 below, cumulative area with number of pixels against grey value is plotted. Two tangent lines are drawn from lower and upper linear segments of the cumulative curve, and the intersection of the two lines represents the location of threshold value.

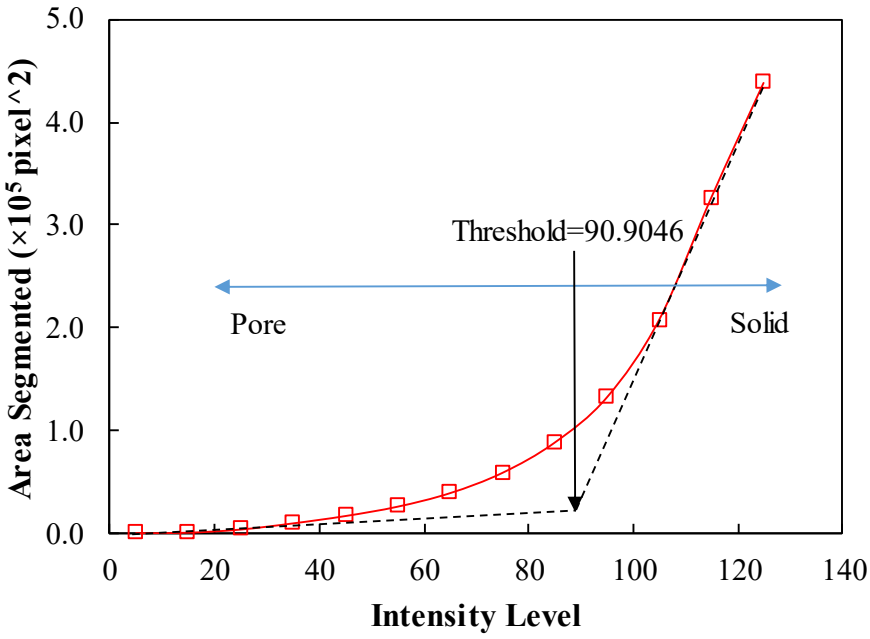

Figure 3.2 Critical point method in finding good estimate for the pore threshold level

Although this method can provide a reliable estimation of threshold value, brightness of images can sometimes cause true critical point being slightly over or underestimate. Therefore further manual adjustment may be required for poor quality images. In this study, threshold value is determined first by drawing tangents from cumulative area curve, then manually adjusted until pore features are satisfactory revealed in figure.

3.3.4 Porosity Estimation

The image analysis is conducted by using an image process software package “Fiji”, a distribution of ImageJ which has many functional plugins for scientific image analysis. The acquired images are first cropped into a desired dimension with 1024 X 768 pixels. Then a threshold intensity is determined using critical point method. As mentioned in previous section, a threshold value of intensities is estimated in order to distinguish pores from solid phases. The pores filled with epoxy resin appear dark where solid phases show brighter intensities in an image. Therefore, pixels with intensity level lower than threshold value will be defined as pores whereas the pixels with higher intensity level are defined as solid. By applying threshold value, cropped image is transformed into a binary image, as shown in Figure 3.3 (a) and (b). The obtained binary image represents pore regions in black and solid phase in white.

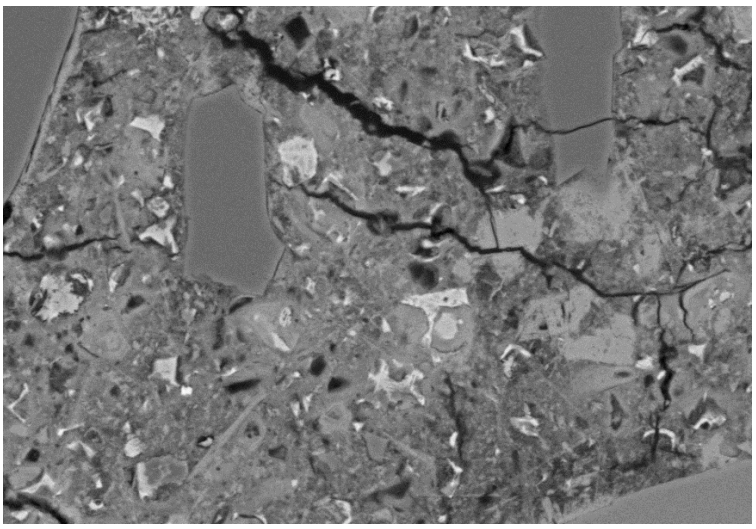

Figure 3.3 (a) 8-bit grey scale image of a mortar specimen

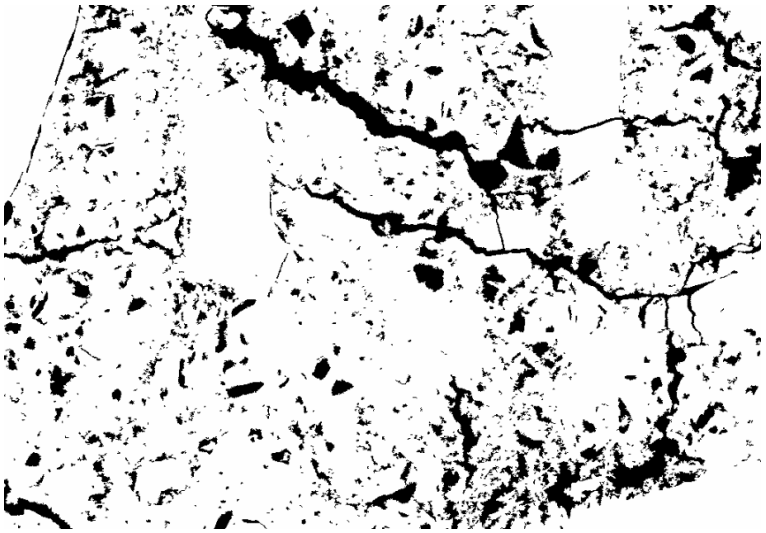

Figure 3.3 (b) Binarized image of a mortar specimen

In order to conduct reliable porosity computation, 12 to 15 images were taken for each sample at magnification of 400X. The pore fraction of a single image determined by counting black pixels in binary image and divide it by total pixels numbers. Then the total porosity of a sample can be estimated by the average value of pore fraction of all images taken from this sample. Note that the porosity investigations are conducted on samples heated at three different heating rate to three different target temperature. It is essential to examine the effect of heating condition to porosity from low to higher target temperatures. Note that poor images only contain large cracks or sand grants are eliminated for the quality of sampling during the analysis of total porosity.

3.3.5 Pore size distribution

The pore size distribution of mortar specimens are identified using image analysis. However, because of the interconnected pore nature and micro-cracks resulted from thermal damage, it is difficult to identify single pore sizes without further qualify the image. Therefore, a qualification process on the already binarized images is necessary in order to obtain accurate and reliable pore size distribution measurements (Muhammad 2018, Scrivener 1989). This work uses Morphological Opening Operation to transform binary images to further proceed with the analysis.

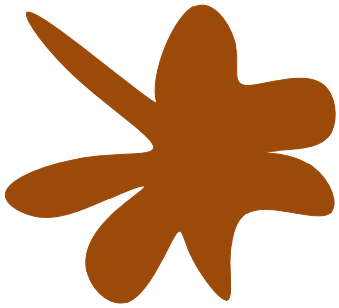

Figure 3.4 (a) Original object

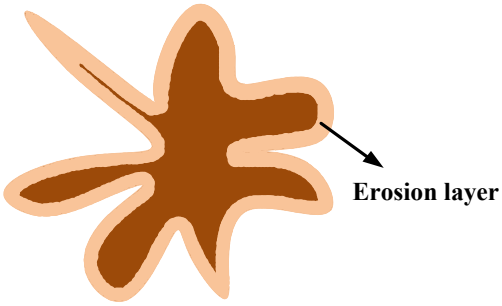

Figure 3.4 (b) In erosion process, a thin layer is removed from the object

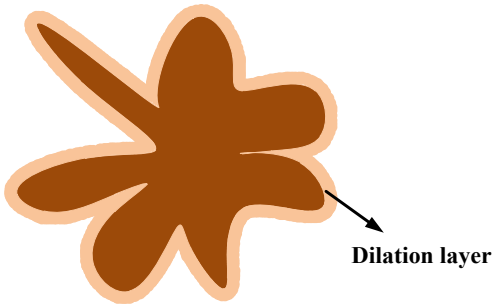

Figure 3.4 (c) In dilation process, a thin layer is added to the object

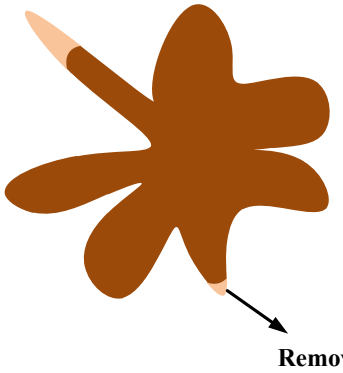

Figure 3.4 (d) In an opened image, the object is dilated from the eroded image

Opening method estimates pore size distribution based on two mathematical morphological transformations: erosion followed by dilation (Scrivener 1989). In this method, a concept of structuring elements is introduced. The effects on a binary image are described in Figure 3.4. Structuring element is a disk shaped element with specified configuration. During erosion transformation process, a layer with width smaller than the configuration of structuring element is removed all the way round inside the original object, as shown in Figure 3.4(b). As a result, the portions of image features with minimum dimension less than the configuration the structuring element are removed (Scrivener 1989). On the other hand, a small layer with same width is added all the way round outside the original object during dilation process. This process fills disconnected regions during transformation, as shown in Figure 3.4(c). After overall processing, complex features such as interconnected pores and micro-cracks having sizes smaller than the current configuration of structuring element are eliminated. The effects of opening operation on an already binarized image are shown in Figure 3.5. Then pore size distribution of mortar specimen is estimated by using a sequence of structuring element with increasing sizes. The sizes of structuring elements are defined as pores sizes of a mortar specimen. At the end of the opening transformation process, the pixel count of pores normalized with respect to the total pixels is recorded (Muhammad 2018). Then, pore size distribution of a mortar specimen from one single image can be presented by a plot of cumulative pore fraction against structuring element sizes.

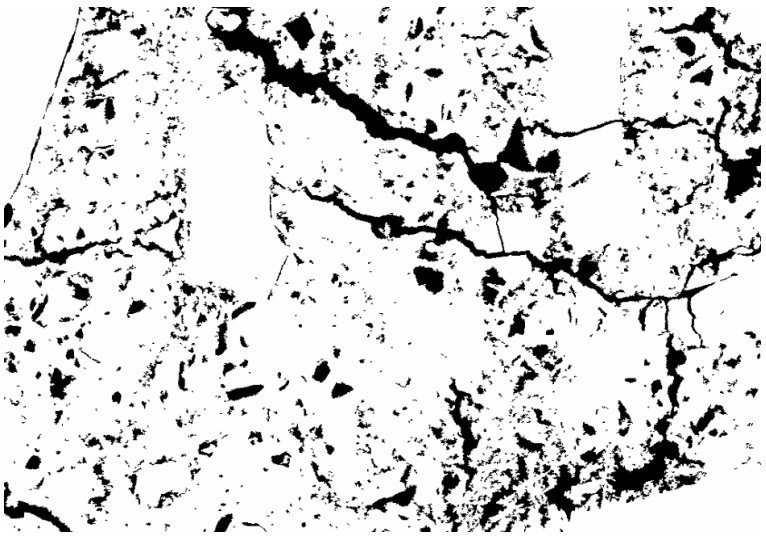

Figure 3.5 (a) binary image of a mortar specimen without performing opening transformation

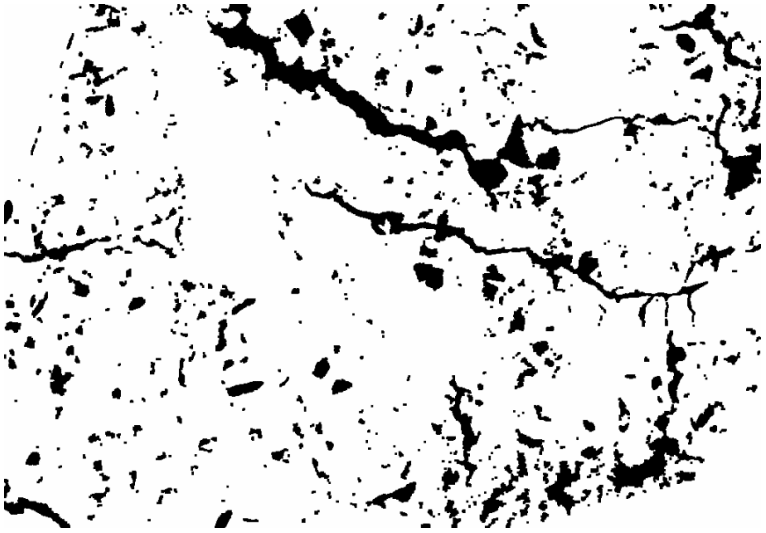

Figure 3.5 (b) binary image of a mortar specimen after one single step of opening operation

Although image analysis using BSE is extremely valuable in studying pore size distribution of cement based systems, limitation still exists in providing accurate measurements. Scrivener (2004) mentions that BSE images gives 2D image of a 3D microstructure, the section of surface will not pass equatorially through all pores. Therefore a distribution of pores size in 2D will be underestimated towards smaller pores since the smaller pores can be a part of large pores. Nevertheless, BSE image analysis is still a powerful method in achieving reliable measurements of pore size distribution.

3.3.6 Fractal Dimension

The measurements of fractal dimension in this study describes the complexity level of pores and also characterize pore distribution patterns at different heating rates. Fractal dimension of pores is estimated by using box counting method on a binary image of a mortar specimen surface. This method involves a sequence of grids having a different cell size, and is placed over the image being examined. Then, the cells covering objects in binary image are counted (Saouma 1994).

In this study, the procedure of box counting was adopted from Muhammad (2018)'s work in determining the pore fractals. The image is first covered by grids with known sizes. Then the

number of grids covering the pore pixels was counted. Next, the size of grids or boxes covering the portion of pores were gradually reduced and corresponding numbers of boxes were counted. As shown in Figure 3.6, the fractal dimension was determined from a log-log scale plot of number of box counted with respect to box size. The absolute value of the line slope was the fractal dimension of pore space from a single image. Note that a linear relationship indicated pore space was said to be fractal within the specified range of box sizes (Saouma 1994). The constant slope indicated the pore features were self-similar. As mentioned earlier in section 2.5.3, self-similarity is the hall mark of a fractal surface. Russ (1992) categorized fractal surfaces into classes, where dense objects having distribution of holes or pores with a fractal structure can be defined as pore fractals. Therefore the porous phase within the mortar can be described using fractal geometry.

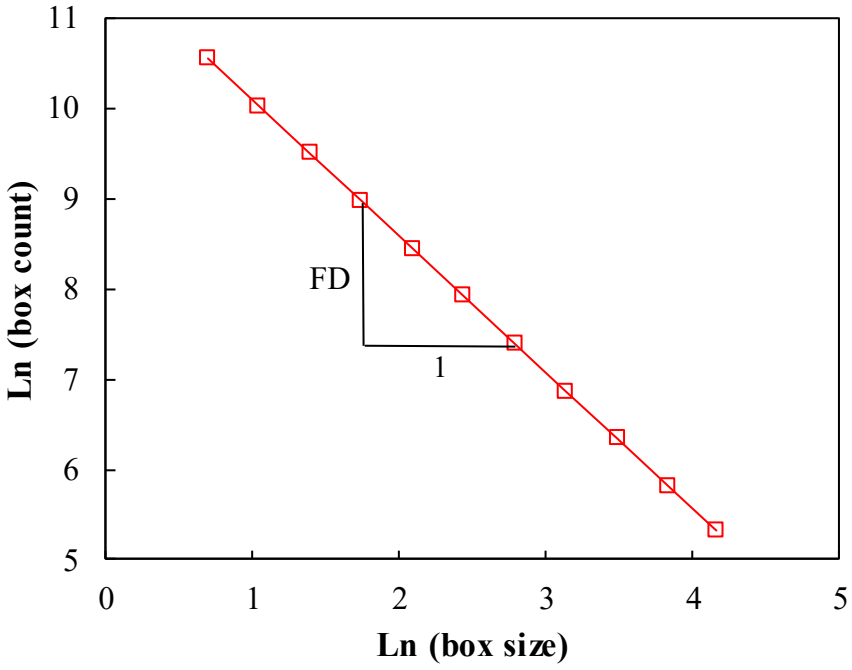

Figure 3.6 Determination of fractal dimension (FD)

3.4 Discussion

The results of total porosity, pore size distribution and fractal dimension against heating rate

and target temperature are presented in this section. In addition, the influence of microstructure change to thermal constants are also discussed.

3.4.1 Porosity

The total porosity of both NSM and HSM specimens with respect to heating rate at different target temperatures are presented in Figure 3.7 below. As other studies have already proved in their results, total porosity of cement based material increases as temperature rises (Chan et al 2000b, Noumowe 2005, Rostasy 1980, Tsimbrovska 1997 and Zhang 2009). At elevated temperatures (up to 400°C), the increase in total porosity of mortars can be caused either by dehydration of capillary pore water or by loss of water molecules chemically bounded in AFT and C-S-H phases (Muhammad 2018). When water evaporates, it transform into steam and causing pore pressure to build up inside voids. As the pressure overcome the tensile strength of mortar, micro-cracks start to propagate from weakened spot such ITZ. This phenomenon contributes more in higher temperatures. As one can see relatively higher increase of porosity in both NSM and HSM figures.

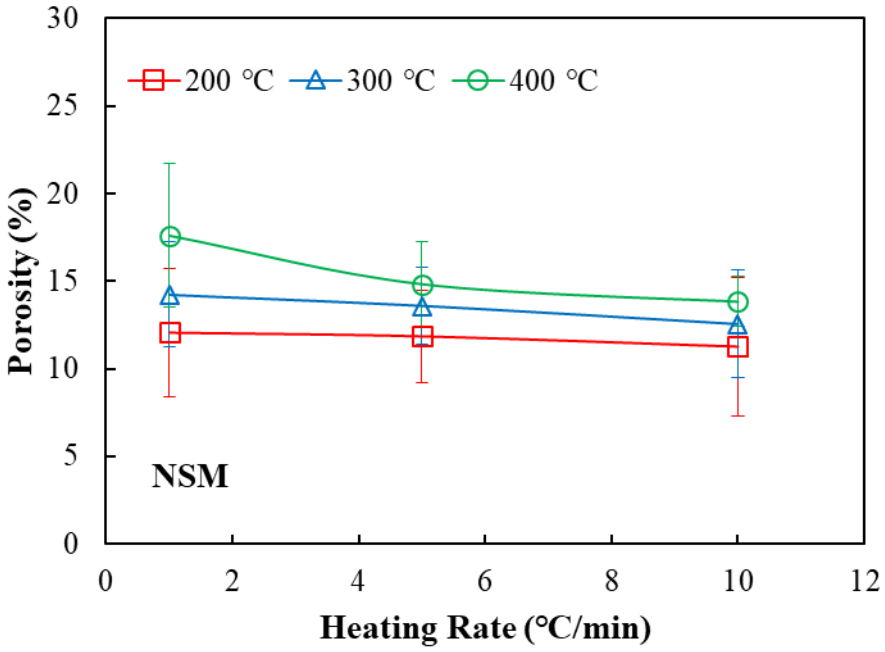

Figure 3.7(a) Effect of heating rate on porosity of NSM at elevated target temperatures

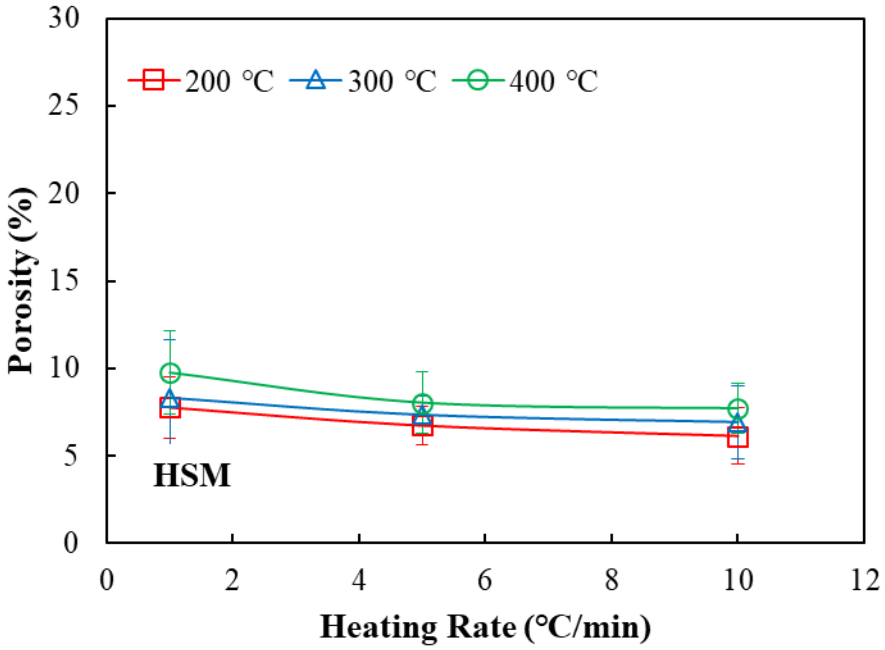

Figure 3.7(b) Effect of heating rate on porosity of HSM at elevated target temperatures

In Figure 3.7 (a) and (b), total porosity of both NSM and HSM show decreasing trend against heating rate to all final temperatures. This is because temperature rise associated porosity change is a continuous process which increased with increasing in temperature and exposure time (Zhang 2009). When mortar specimens are heated under high heating rate, the exposure time for mass transfer is limited. On the other hand, the lowest heating rate provide sufficient time for water to escape from the inside of mortar specimens and therefore the resulted porosity levels are higher. In this study, the exposure time is 10 times higher at lowest heating rate comparing to the highest. The reason that both figures do not show significant drop in porosity at the heating rate may attribute to a build-up of pore pressure. Since the time for mass transfer is limited in this situation, high pore pressure may cause additional micro-structural cracks which lead to increase in void fractions. If the mortar specimen is exposed in high temperature longer enough, a hygric equilibrium state can be reached such that the specimen no longer loss water under this temperature. Hygric equilibrium state can be reached faster in higher heating temperatures, which means the rate of mass transfer speeds up in higher temperatures. This phenomenon is also reveal by the rate of porosity change in both NSM and HSM figures. As

indicated by plots, the rate of porosity change against heating rate tends to increase with heating conditions to higher target temperatures.

3.4.2 Pore size distribution

Pore size distribution of each mortar specimens are determined using morphological opening method as mentioned in 3.3.5. After each step of opening transformation process, pores smaller than the size of structuring element are removed. The sum of area fractions of pores being removed in each steps of the operation are obtained and thus a cumulative area fraction of pores with respect to structuring element size (or pore size) can be plotted in the end.

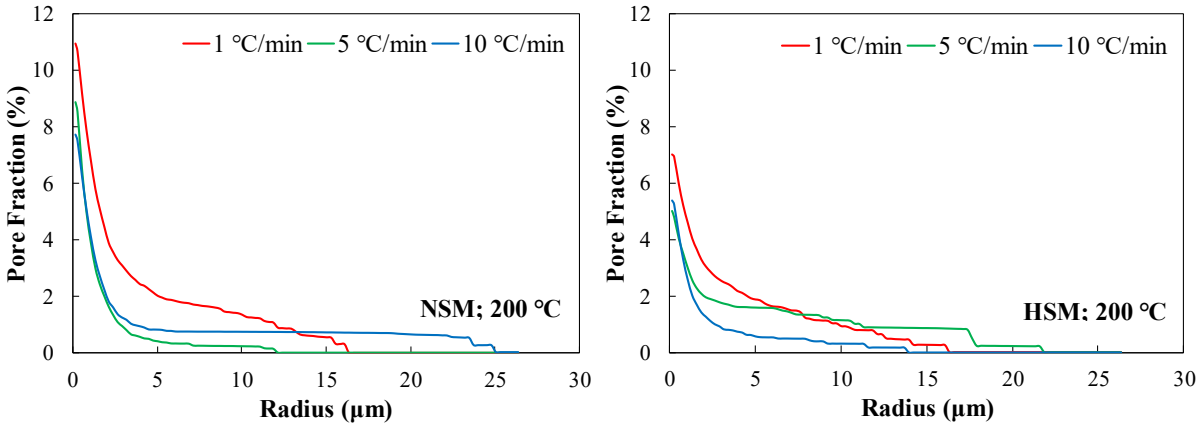

Figure 3.8 (a) Pore size distribution of NSM and HSM heated to a target temperature of 200°C

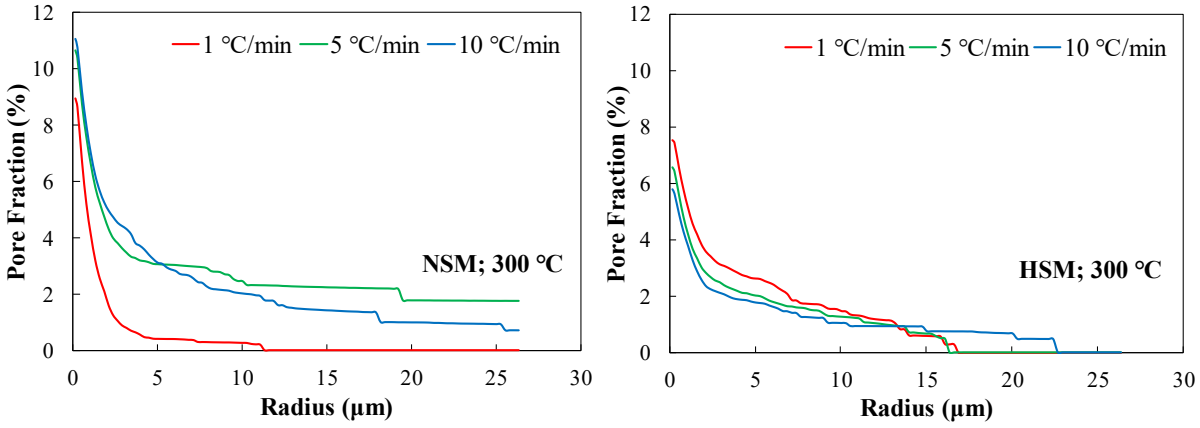

Figure 3.8 (b) Pore size distribution of NSM and HSM heated to a target temperature of 300°C

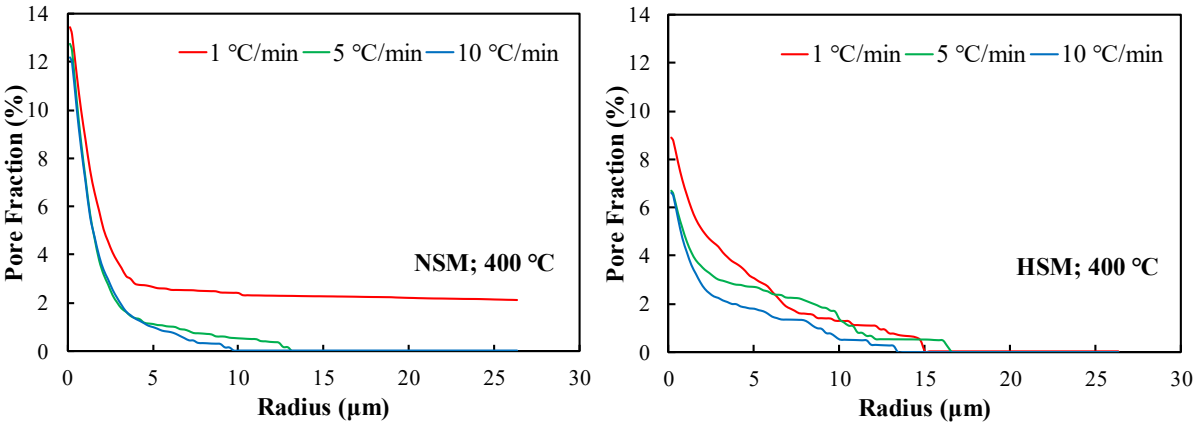

Figure 3.8 (c) Pore size distribution of NSM and HSM heated to a target temperature of 400°C

Figure 3.8 shows the pore size distribution of mortar specimens heated to 200, 300 and 400°C at 1, 5 and 10 °C/min heating rates. Results were acquired by combining the data from images at magnification of 400X and 800X, thus the detected minimum pore size can reach as small as 0.14µm in radius. It can be notice that the overall pore size distribution of mortar specimens heated at 1 °C/min rate are observed much higher than other two heating rates. This increase in pore sizes can be attributed to sufficient heat exposure time provided at low heating rate. The plots also show similarities of the mortar specimens heated at 5 and 10°C/min rates in pores sizes and total detectable porosity level to all target temperatures. It can be explained by their less dispersed heating time.

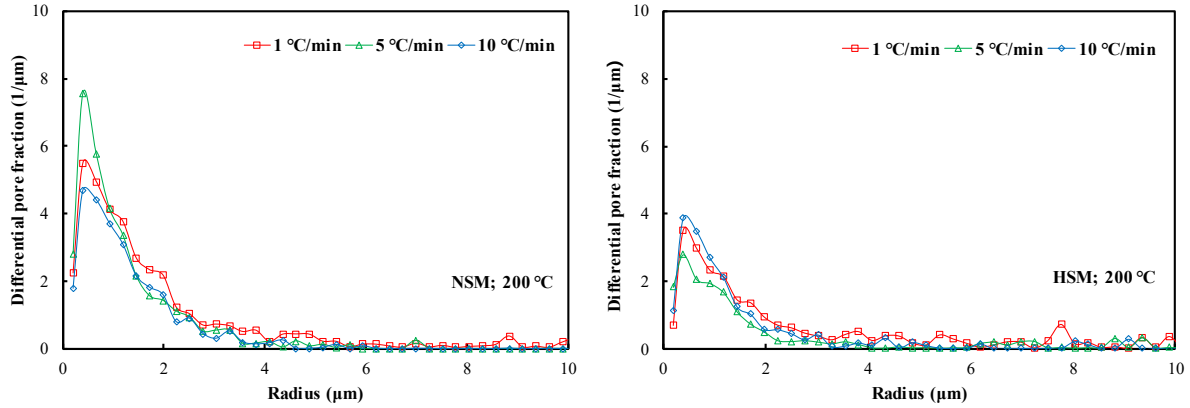

Figure 3.9 (a) Differential pore size distribution of NSM and HSM heated to a target temperature of 200°C

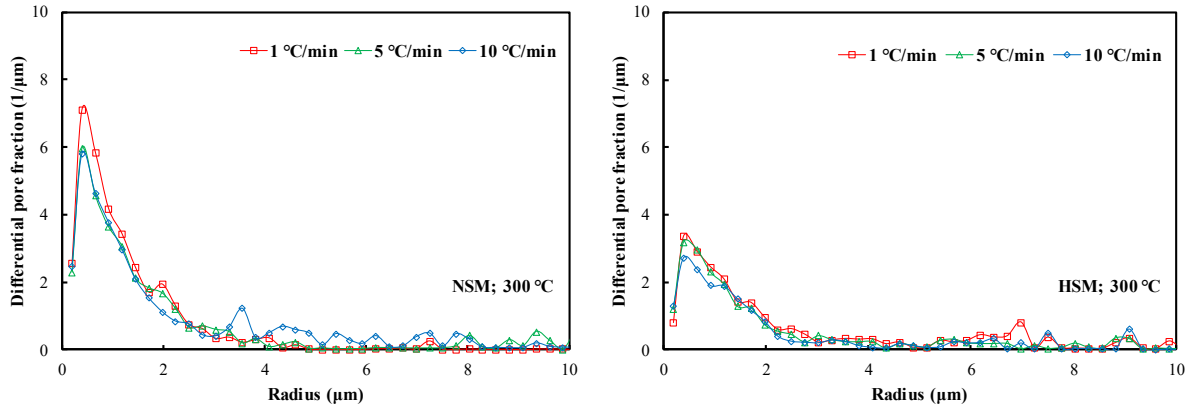

Figure 3.9 (b) Differential pore size distribution of NSM and HSM heated to a target temperature of 300°C

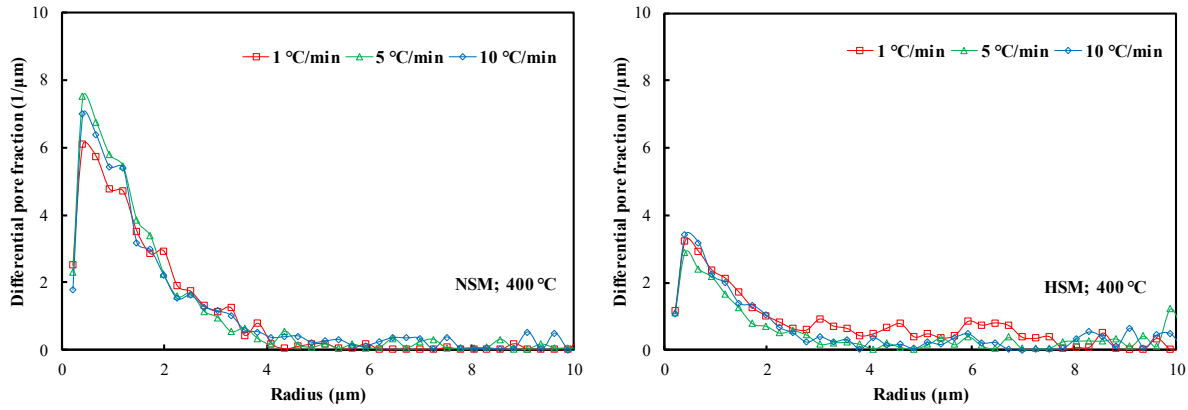

Figure 3.9 (c) Differential pore size distribution of NSM and HSM heated to a target temperature of 400°C

Figure 3.9 (a) to (c) present differential pore size distribution of mortar specimens heated to a desired target temperature at different heating rates. The critical pore radius is found at 0.4 µm for all tested specimens. There is no observation of any noticeable shifting of critical pore size from either variation of heat rate or targeting temperature. It may be attributed to limited soaking time after heating process which could cause major shift of pore sizes. Another interesting fact can be observed from the plots, Figure 3.9 (a) indicate that the effect of heating rate to pore size coarsening is limited with a low targeting temperature for both mixes. As the targeting temperature rises, effect of heating rate change becomes more critical to pore size coarsening. Since the heating time required to reach the target temperature is more dispersed

with different heating rate, the amount of crystallized water evaporating from C-S-H is also dispersed, leaving enlarged pores. Because of the addition C-S-H content, the effect of heating rate on pore size distribution of HSM is more significant comparing to NSM. It is also noticeable from Figure 3.9 that lowering heating rate increases pore fractions toward large pores. Since HSM is brittle and less permeable, this pore size enlargement can definitely mitigate induced internal thermal stress at certain point.

3.4.3 Fractal Dimension

Fractal dimensions (FD) of both NSM and HSM specimens heated at different heating rates are shown in Figure 3.10. As mentioned in section 4.3.5, the results of FD are determined using box-count method. The FD value shows a positive relationship with heating rate for both NSM and HSM. For NSM, the increase in FD over heating rate is quite smaller comparing to HSM. FD value changes from 1.47 at 1°C/min to 1.49 at 10°C/min rate with only 0.02 in difference. However, this difference in FD value between the highest to the lowest heating rate is recorded as low as 0.014 when the final target temperature rises to 400°C. On the other hand, the increase in FD value resulted from heating rate change is relatively higher for HSM. It can be attributed to micro-cracks from induced damage after exposing to heat. Similarly, the change in FD value over heating rate drops with an increase in final target temperature for HSM. For instant, the difference of FD value between the highest and the lowest heating rate is 0.11 with exposure temperature of 200 °C. Then, it drops to only 0.05 as the target temperature increase to 400 °C. The results indicate that heating rate can have more impact on fractal dimension at lower temperature.

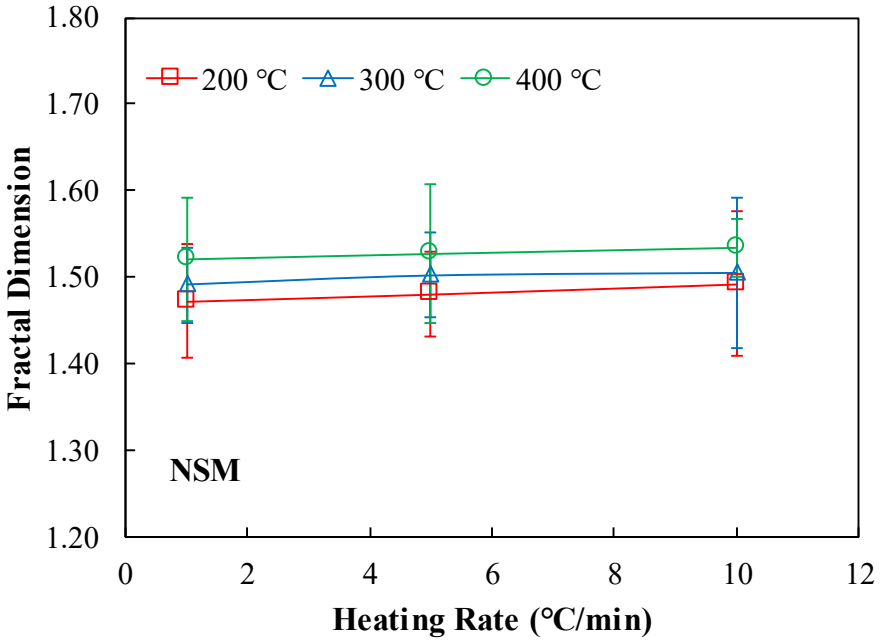

Figure 3.10 (a) Fractal dimension of NSM heated at different heating rates

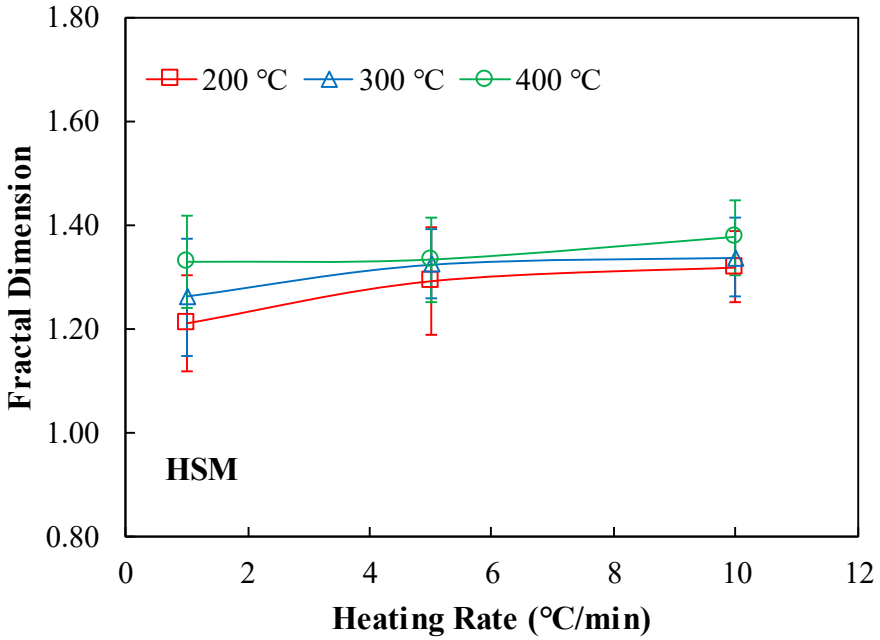

Figure 3.10 (b) Fractal dimension of HSM heated at different heating rates

The flatten slope of FD curve at high target temperature can be explained through largely increased porosities. Yu and Li (2001) have developed mathematical expression that predicts a positive relationship between FD and porosity of a material based on the experimental results.

The increasing trend of both FD and porosity level against temperature provides a fair agreement to their study. However, the results from foregoing section show a contradictory information that the porosity level decreases as heating rate rises. This discrepancy can be attributed to increasing in micro-cracks caused from build-up of pore pressure at higher heating rates. Note that fractal dimension describes the shape irregularity of an image (Muhammad 2018). The increase in micro-cracks results higher irregularity of structure shape, which are adequate for overcoming the influence of porosity level to FD. In high temperatures, the pore size coarsening effect becomes much significant to the porosity, and therefore the increase in FD value is less conspicuous. Note that heating rate gives more impact on FD for HSM due to its low permeability. This observation also indicates cement based materials with low ductility has less resistance to heat at higher heating rate.

3.5 Conclusion

The microstructure of mortar mixtures plays an important role on heat and mass transfer under exposure of heat. This study takes close observation of pore structures using BSE image analysis, and develops better understanding on how the mortar behaviors under different heating process at the micro level. The microstructure of HSM appears to be more sensitive to heating rate comparing to NSM Based on experimental investigation combined with mathematical analysis, the following key findings regarding the pore structure of mortar under different heating conditions can be concluded:

- The porosity of both normal and high strength mortar increases with an increase in final exposure temperature. However, the porosity drops for an increase in the heating rate. This is likely due to the limited exposure time provided for mortars heated at higher rates, where the pore coarsening is a continuous process at elevated temperature. In addition, the pore coarsening process accelerates as the final targeting temperature increases;
- The variation of heating rate has limited effect on critical pore radius. Moreover, the effect of heating rate tends to be conspicuous on pore size distribution as the final targeting

temperature increases;

- There is an increase in fractal dimension of pores as temperature increases, which agrees with the similar findings from prior work;
- The fractal dimension of NSM and HSM increases with heating rate. However, the this trend is more obvious for lower target temperatures. It appears that the influence of pore coarsening becomes more dominant on fractal dimension.

Chapter 4 Thermal Characteristics of Normal and High Strength Mortar at High Temperatures under Different Heating Rates

4.1 Introduction

Although it is the most common building material today, the change in thermo-physical properties of concrete under elevated temperatures continues to draw attention. While concrete is not combustible, it has good fire resistance comparing to other building materials (Shoaib et al., 2001). When exposed to elevated temperatures, spalling phenomenon of concrete is the most significant concern in its fire performance. Multiple studies have shown that concrete with lower permeability tends to have higher risk of spalling (Ali F. A et al 2001, Chan Y. N. 1999, Kodur 1998). In fire, the heating rate of concrete varies under different exposure type and fire source (Hu et al., 2011, Tran and White 1992). For heating rate higher than 1°C/min, the occurrence of explosive spalling happens more frequently in high strength concrete (HSC) than in normal strength concrete (NSC). The thermal gradient is induced during the heating process on account of its relative low thermal conductivity and high specific heat. The spalling phenomenon occurs at the time when thermal gradient inside concrete specimens reaches maximum (Phan, 2001). The results have shown that the induced strain energy from thermal gradient is one of the key factors that govern spalling phenomenon to occur. Therefore the study conducted by Le et al. (2018) presented the fire performance of concrete structures taking the temperature gradients into account.

In previous studies, both physical and chemical changes due to loss of water that occurs at different stage of the heating process, and the resulting changes to the thermal properties of mortar are described (Al-Sibahy and Edwards 2012, Shoaib et al., 2001). As noted earlier in this thesis, the solid constituents of paste contains approximately 65% of C-S-H phase, while other hydration products like sulphoaluminate and CH occupies the rest of the volume. In the event of heating, free water in capillary pores starts to evaporate above 100 °C and chemical decomposition of hydration products occurs soon after. The AFt phases start to lose water

molecule at a temperature range of 70 to 110°C (Hager 2013, Zhou and Glasser 2011). Dehydration of C-S-H takes place between 100-300°C. However, unhydrated cement can then react with the released water molecules to produce extra C-S-H upon heating. Thereafter, calcium hydroxide loses water above 400°C, decomposing into calcium oxide and water vapour. In addition, Kim et al. (2003) reported that the temperature of exposure affects the thermal conductivity significantly. Kodur (2003) described the effect of temperature on thermal properties of HSC. The thermal conductivity decreased with an increase in the temperature, while the specific heat (thermal capacity) remained relatively flat below 600 °C. Similarly, recent research on thermal properties of self-consolidating concrete also observed a decrease in the thermal conductivity with an increase in the temperature up to 400°C (Khaliq and Kodur, 2011). The drop in thermal conductivity was likely due to the decrease in the moisture content inside concrete. As the temperature rises beyond 400°C, decomposition of calcium hydroxide brings in additional moisture and causing a small rebound of thermal conductivity. Furthermore, Kodur and Khaliq (2010) concluded that the effect of polypropylene and hybrid fibers on thermal conductivity were minor at heating rates of 3~4°C/min, however they increase the specific heat at temperatures higher than 400 °C.

From the present research summarized above, the thermal properties of various type of concrete and mortar have been studied under different temperatures. However, the heating rate is an important parameter causing spalling to occur, and its influence on thermal properties remain to be understood.

4.2 Objectives

This chapter focuses on the effect of heating rate on thermal constants of mortar specimens using the transient plane source (TPS) method. In order to further understand the thermal behaviour of mortar, both normal strength mortar and high strength mortar are examined in this work under different heating rates up to a target temperature of 400°C. Thermal properties including thermal conductivity and specific heat are measured. The relation between thermal

constants and weight loss are also monitored. Two distinct mixtures were designed, widely varying in their composition and mechanical outcome. Together, this represents a fresh experimentalstudy to measure thermal constants under variably heating rates. The data produced here connects the thermal behaviour of concrete with different heating rates.

4.3 Experimental procedure

4.3.1 Specimen Preparation

Both mortar mixtures namely, the NSM and the HSM were prepared with a rotary high speed mixing machine as shown in Figure 4.1 below. The mixing pan rotated in the opposite direction of mixing blade so that the constituent materials could be blended properly and more efficiently. The control panel on the right hand side allowed variation on rotational speed according to different user purposes.

Figure 4.1 High speed mixing machine used for specimen preparation

Before mixing, the Portland cement and supplementary cementing materials (if any) and

blended silica sand were measured and pre-mixed manually using a scoop in the mixing pan under dry condition. A designed amount of water with high range water reducing admixture was added and mixed mechanically for 10 minutes. Then, the PET fibre was gradually added through a small hole in the cover, while the mixer was still running. Note that fibres were added to provide integrity to the resultant mixture, even though this study did not evaluate the their effect upon the thermal constants. After fibre addition, mixing was continued for another 10 minutes.

The two mortar mixtures were cast in 75 mm X 150 mm cylinders and 50 X 50 X 225 mm prism, and then mechanically vibrated for 5 minutes based on ASTM C192/C192M—16a. The mortar specimens were cured in a room with controlled humidity and temperature of 23°C. Accelerated hydraulic curing was introduced at 24 h. The procedure was similar to ASTM STP 169 D Procedure B, but with specimens de-molded and immersed in hot water at 95°C. After 3.5 h of hydraulic cure in water bath, the specimens were stored in a humidity room till the day of testing. At the age of 6 days, the cylinders were air dried at room temperature for 24 h and then capped using sulphur following standard as per ASTM C617/C617M—15. The 7 day compressive strength was tested following ASTM C39 standard procedure by MTS Compression Test Machine at loading rate of 1 mm/min, and the results are listed in Table 3.2.

4.3.2 Experimental Detail

In order to measure thermal constants, a 50 mm X 50 mm X 225 mm sized prism was sliced into three pairs of test specimens with 25 mm thickness. Since the porosity and permeability of mortar is strongly affected by moisture content, pre-drying is required in order to obtain consistent and reliable measurements (Kearsley 2001). Both NSM and HSM specimens were oven dried at 100°C for around 24 hrs. Each pair of specimens was used to measure thermal constants at 1 °C/min, 5 °C/min and 10°C/min heating rate respectively. The target temperatures were 200°C, 300°C and 400°C. This maximum peak temperature is chosen to avoid potential risk of explosive spalling on high strength mortar.

Thermal constants were measured by employing a hot disc thermal analyzer “TPS 1500”

following ASTM D7984. The high temperature resistance wires were used to connect thermal sensor inside a programmable furnace to the analyzer. A mica-insulated sensor with radius of 9.7 mm was sandwiched between two sliced mortar specimens in the holder, which were exposed to high temperature in the furnace as shown in Figure 4.2 (a) and (b). The sensor was tightly attached to interfacial surfaces of mortar specimens.

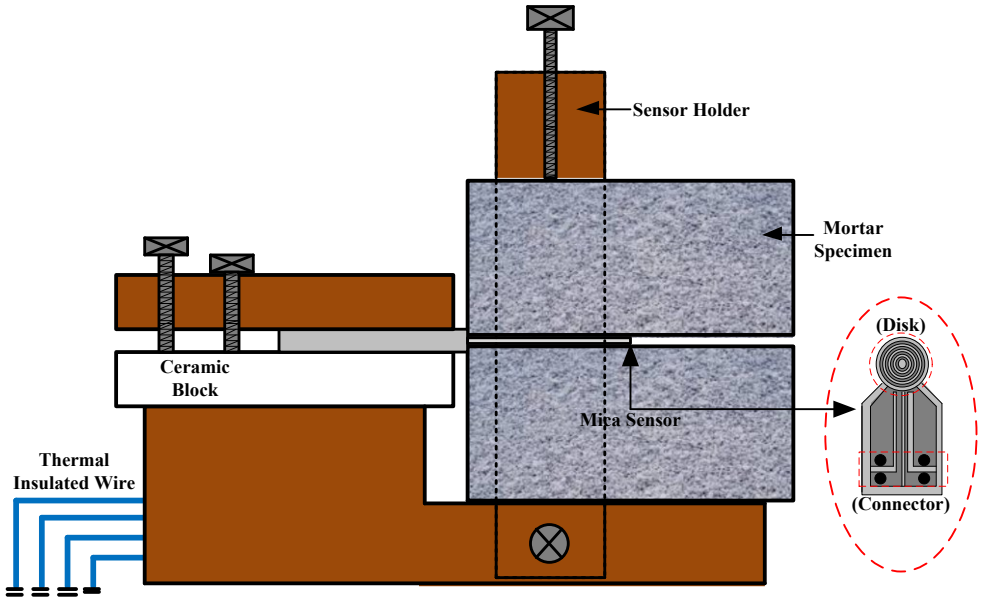

Figure 4.2 (a) Mica-insulated sensor were positioned in the middle of sliced mortar specimens

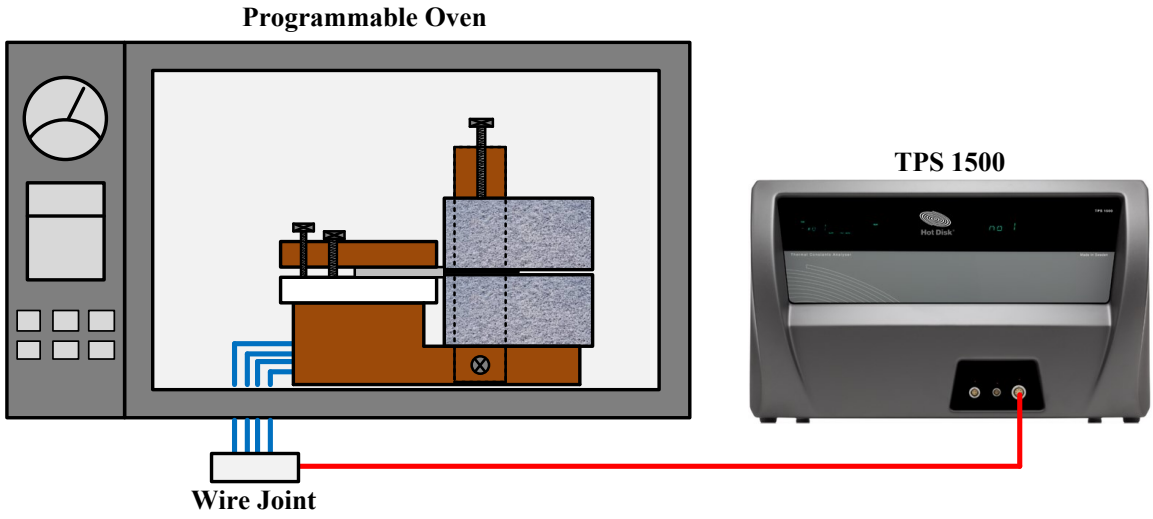

Figure 4.2 (b) Specimen is loaded and ready for test

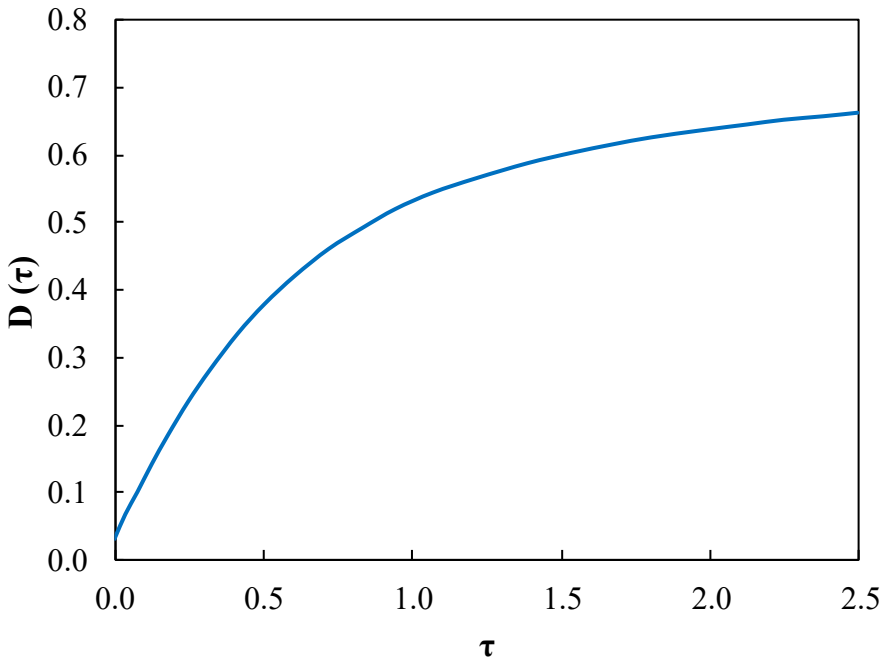

Figure 4.3 Plot of a dimensionless function D (τ) with an increase in τ

This method is known as the transient plane source (TPS) method. During the measurements, a constant current is generated in the sensor to heat up. The temperature increase of the metal disk inside mica sensor is highly dependent on the tightly attached mortar specimens. Therefore, the thermal constants can be determined by monitoring this temperature increase for a small amount of time at target temperatures (Zhao et al 2016). In this research work, 80 seconds is selected for the measurements. The theoretical expression for the temperature increate at the sensor surface ΔT as a function of time is expressed as follows:

$$\Delta T(\tau) = \frac{Po}{\pi^{1.5} rk} D(\tau) \qquad (4.1)$$

$$\tau = \sqrt{\frac{t\alpha}{r^2}} \qquad (4.2)$$

Where ΔT is temperature increase, Po is the total output power, r is the radius of the outermost ring of sensor, k is the thermal conductivity of specimen, t is time, α is thermal diffusivity and D (τ) is a dimensionless function of τ, which describes heat conducting pattern of the sensor (Bouguerra et al 2001). The plot of D (τ) as an analytical expression of the time dependent increase is shown in Figure 4.3. Since t is the selected value and ΔT is measured during the

measurement, the inverse of thermal conductivity k then can be calculated by involving the above two equations. In this study, both thermal conductivity and specific heat are focused.

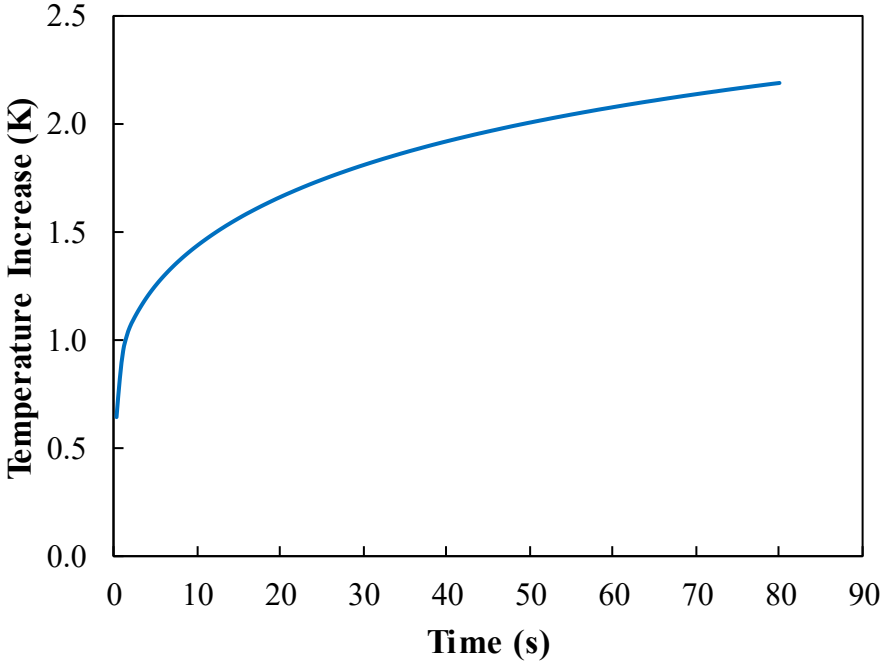

Figure 4.4 Typical temperature increase recorded in TPS system

There are several factors that can affect the result of thermal measurements, such as variation in test temperatures, thermal contact resistance between the sensor and specimen surfaces as well as the measured power input being influenced by the electrical isolation of sensor. The biggest challenge in this study is unsteady testing temperature. The programmable oven used for this experimentation requires additional time to stabilize after it reaches programmed maximum target temperature. The typical temperature-time history curve recorded using TPS is reveal in Figure 4.4. If the oven temperature is not steady during the measurement, large fluctuation will appear on the curve, resulting incorrect measured thermal constant. In addition, decomposition of hydration products in mortar specimens appears to disturb the TPS measuring system. Mica sensor encounters hard time in balancing under higher target temperatures (above 300°C) if the soaking duration is not sufficiently long. Note that with higher target temperatures, both oven temperature and mortar specimen required longer time to stabilize for proper measurements. As a result, the measurements were taken approximately 30 minutes after the

furnace first reaches target temperatures of 300°C and 400°C. The heating curves and the following soaking periods are shown in Figure 4.5 below. This soaking period was selected by trials of measurements, which is the minimum time required to obtain consistent thermal constant results. In addition, the weight loss of specimens is also monitored at the same time.

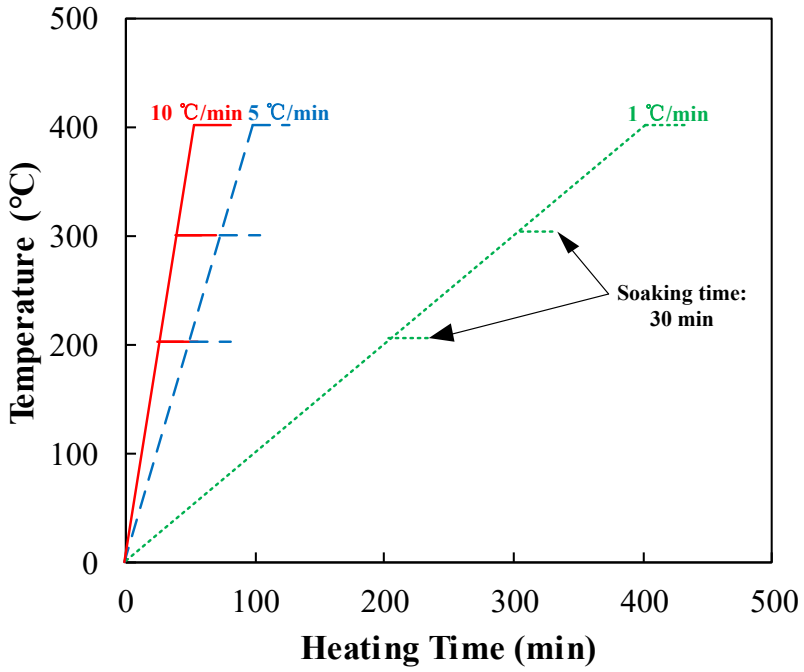

Figure 4.5. Heating cycles used to heat mortar samples

4.4 Results and Discussion

The measured weight loss, thermal conductivity and specific heat are presented in the following sections. The result data of thermal constants will be discussed in the aspect of physical change and microstructure to the thermal behaviour of mortar specimens due to heating rate change at high temperatures.

4.4.1. Weight Loss

The monitored weight loss of NSM and HSM are shown in Figure 4.6 below. The results

indicate much higher weight loss of HSM comparing to NSM at high temperatures. It can be attribute to two factors: water amount and addition of silica fume. Although the water to cement ratio of NSM is higher than which of HSM, the amount of water added by weight is greater in HSM. Moreover, the experimental results from Sancak (2008)'s work show generally higher weight loses of concrete containing silica fume. Similarly, Saad (1996) have found 3% increase of weight loss at 400°C with concrete containing 15% of silica fume content.

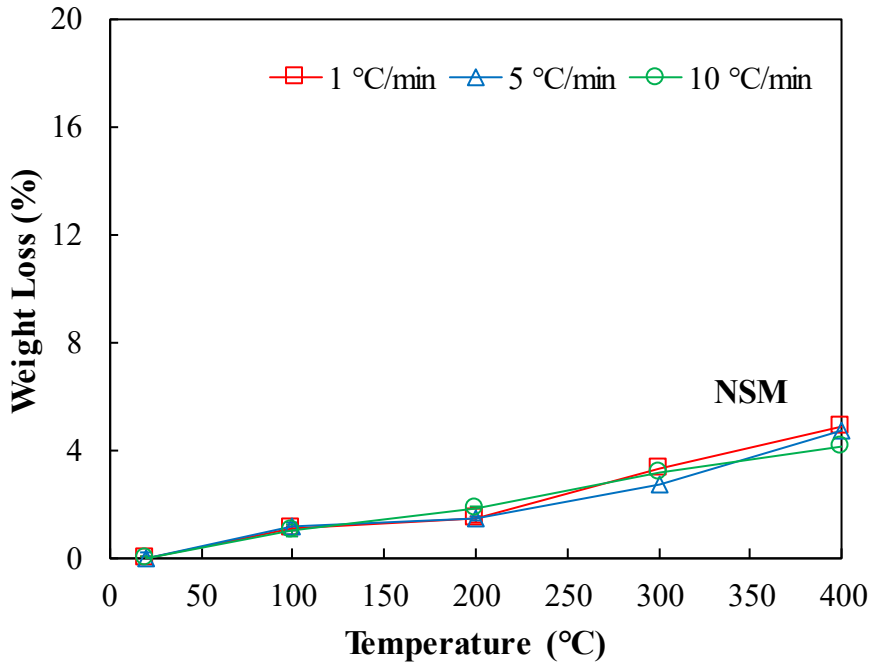

Figure 4.6(a) Weight loss of NSM over temperature

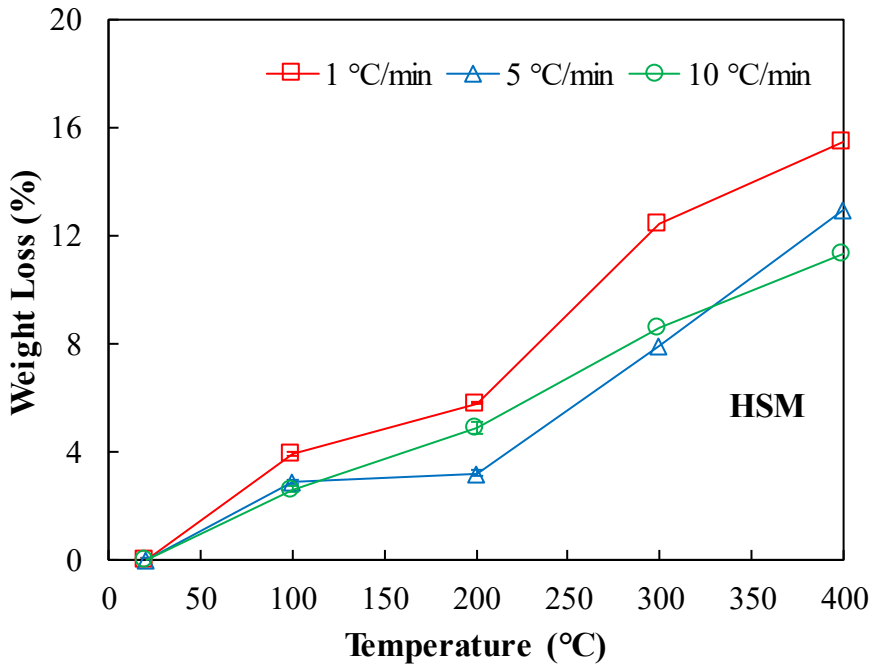

Figure 4.6(b) Weight loss of HSM over temperature

However, the porosity as evaluated from image analysis do not have the same pattern. On the contrary, porosity percentage changes for HSM under all heating conditions are quite smaller than NSM. One of the reasons is likely the increase in pore volume associated with dehydration of capillary pore water, which is not completely revealed in 2D BSE image. As mentioned before, pore sizes can be underestimated since the smaller pores can be actually a part of large pores. Second, HSM has lower permeability and therefore low porosity level comparing to NSM. As temperature rises, pore volume of HSM increases in much smaller scales. Therefore, some pores can be too small to be detected by an image since the BSE image analysis limits the minimum pore size of 0.14μm in radius due to the selected magnification. Nevertheless, with consistent magnification selected in the image analysis on both NSM and HSM, it is still a valuable method in revealing the relationship of porosity change and heating rate.

4.4.2. Thermal conductivity

The measured thermal conductivity of NSM and HSM to heating rate at elevated target temperatures are shown in Figure 4.7 (a) and (b). Both plots show a decrease in the thermal

conductivity for a rise in the temperature. This decrease in thermal conductivity can be related to weight loss concerning decomposition of calcium aluminates combining with evaporation of chemically bounded water in hydrated calcium silicate (C-S-H). Al-Sibahy and Edwards (2012) states that dehydration of C-S-H initiates approximately at 150 °C, and calcium aluminates losses water molecules at approximately 100°C. As expected, Figure 4.5 (a) and (b) show trend of increasing weight loss with increasing in temperature. As bound water evaporates, porosity level inside mortar specimens increases, causing the drop in thermal conductivity. The relationship between porosity and thermal conductivity has been evaluated by dos Santos. W. (2003).

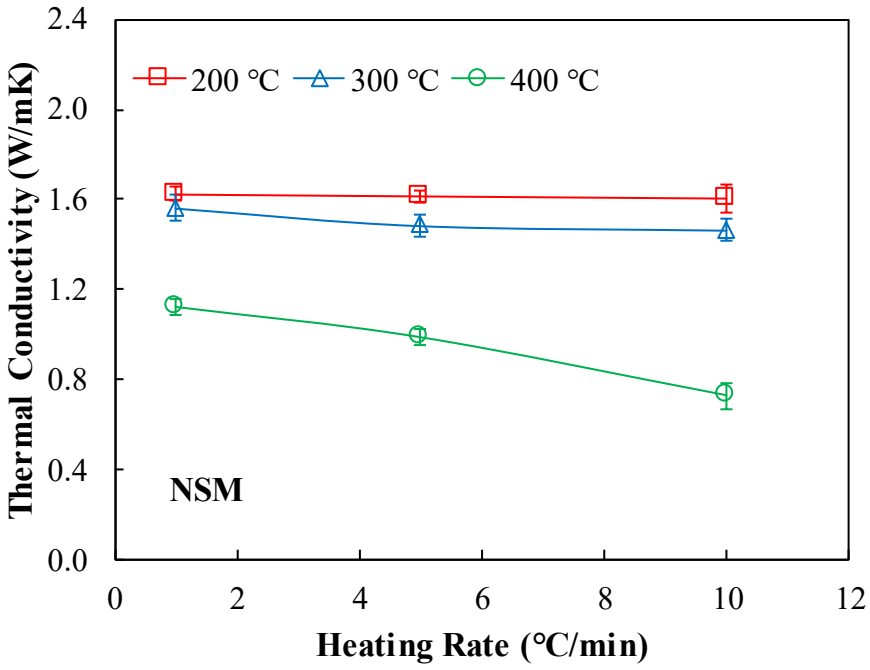

Figure 4.2 (a) Effect of heating rate on thermal conductivity of NSM at elevated target temperatures

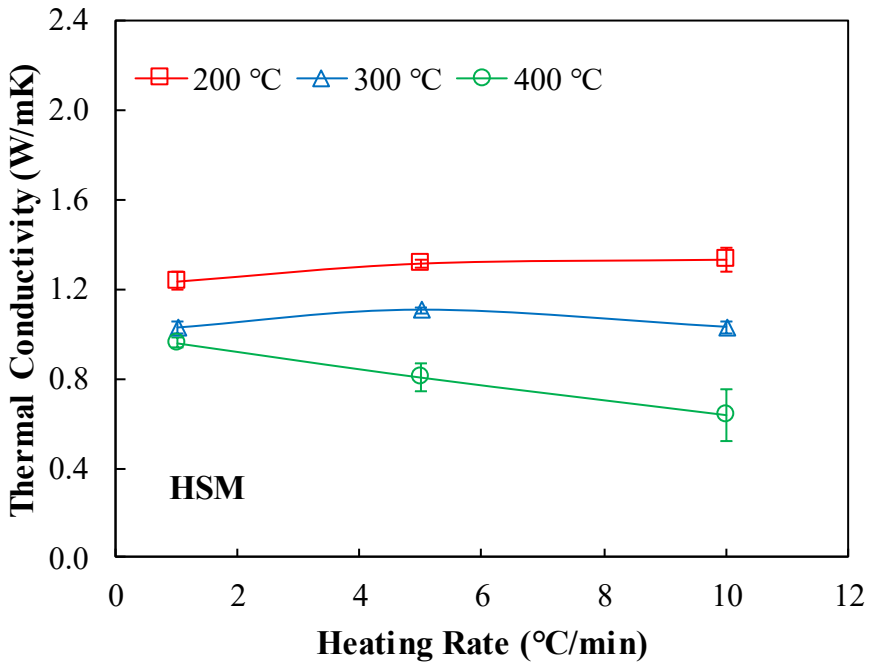

Figure 4.7(b) Effect of heating rate on thermal conductivity of HSM at elevated target temperatures

Figure 4.7(a) displays the decrease in thermal conductivity for an increase in heating rate at all target temperatures for NSM specimens. At lower target temperatures, changing heating rate has little or no effect on the change in thermal conductivity. However, heating rate change becomes significant to thermal conductivity at the highest target temperature. It is apparent that the target temperature also has influence on the relationship between thermal conductivity and heating rate for NSM. However, Figure 4.6 (a) reveals much less total weight loss due to temperature raise in NSM specimens comparing to HSM. Furthermore, this figure also shows negligible difference of total weight loss between all three heating rates. Even at temperature of 400°C, the difference in total weight loss between 1°C/min and 10°C/min is only 0.5%. As the result, it is fair to say that the contribution of porosity to thermal conductivity for NSM at all heating rates is not very significant. The behaviour of thermal conductivity in Figure 4.7 (a) can be mostly attributed to additional micro-cracks resulted from thermal induced pore pressure at high heating rates. In addition to pore pressure, high thermal gradient may potentially be produced between the core and surface of the mortar specimen when the external temperature rises in a fast pace (Kodur 2007). As a result, the thermal stress may cause further physical

damage to the micro-structure of the specimen. These micro-cracks become barriers to preventing heat transfer. Moreover, lattice vibrations of crystal structure in quartz from both fine aggregates and the interfacial transition zone (ITZ) can also influence efficiency of heat transfer. Dos Santos (2003) presented that thermal conductivity of glassy component has a proportional relationship to specific heat which increases with temperature. The specific heat curve of NSM shown in Figure 4.9(a) provides evidence of similar pattern at temperature of 400°C. In this case, the total heating time differences between specimens are greater at 400°C. Therefore the specimen with low heating rate has sufficient time for diffusion of the vibrational energy throughout mortar specimens, causing reduced temperature gradient, and hence higher average thermal conductivity (Dos Santos 2003).

Compare to NSM, thermal conductivity of HSM shown in Figure 4.7 (b) is relative low at all temperatures. This is resulting from about three times less silica sand being used in the mix, and therefore less proportion of quartz is presenting to enhance heat transfer efficiency in HSM specimens. In addition, the plot of HSM shows opposite conductivity trend comparing to NSM at the lowest target temperature. The thermal conductivity gradually increases at heating rate arise. This phenomenon can be explained by porosity level increase caused by high weight loss in HSM. In Figure 4.6 (b), the total weight losses of HSM at 200°C and 300°C are 3 ~ 4 times as much of NSM. As listed in table 1, large proportion of cement and silica fume is used in mixing, resulting in relatively higher C-S-H content and low initial porosity. Since HSM contains higher C-S-H content, amount of crystalized water evaporates during heat exposure will also be great. In addition, low initial porosity indicates low permeability, which reduces the rate of mass transfer inside HSM at higher heating rate. In another words, low heating rate provides a longer time for water to escape from inside, resulting in higher weight loss and increase in porosity. The results from section 3.4.1 show porosity difference at 200°C between the lowest and highest rate is only 0.8% for NSM, where porosity difference is 1.6% for HSM. Moreover, 1°C/min heating rate curve in Figure 4.6 (b) shows much higher level of total weight loss comparing to others. It is also noticeable that the variation of total weight loss between 5°C/min and 10°C heating rates is quite small since the heating time is less dispersed. It is clear

that percentage of porosity difference between heating rates is higher for HSM comparing to NSM. This variation is then reflected in thermal conductivity curves in lower temperatures. As a result, the behaviour of thermal conductivity at low exposure temperatures follows the same trend as porosity. However at 300°C, thermal conductivity curve first increases and then drops at the highest heating rate. This inconsistency can be attributed to low permeability and brittleness of HSM. Large proportion of cement materials are used in mix, resulting in brittle structure and low overall porosity. Therefore HSM has very poor resistance to internal pressures. As mentioned before, a peak evaporation of bonded water from C-S-H occurs around 270°C (Al-Sibahy and Edwards 2012). This sudden increase in pore pressure can cause great damage to micro-structure of HSM. The increase in fractal dimension from Figure 3.10 (b) indicates increased irregularity from additional cracking at both high heating rate and temperture. As the result, the porosity level still shows influence on thermal conductivity at 1°C/min heating rate. However, the combined effect of additional micro-cracks and contribution of quartz to thermal conductivity overcomes the influence from porosity when the heat rate reaches to 10°C/min. This can be attributed to smaller variation of porosity level between 5°C/min and 10°C heating rates. Similar as NSM, the curve at 400°C curve displays an inversed proportional relationship of thermal conductivity and heating rates. This may be attributed to cracking and contribution of quartz.

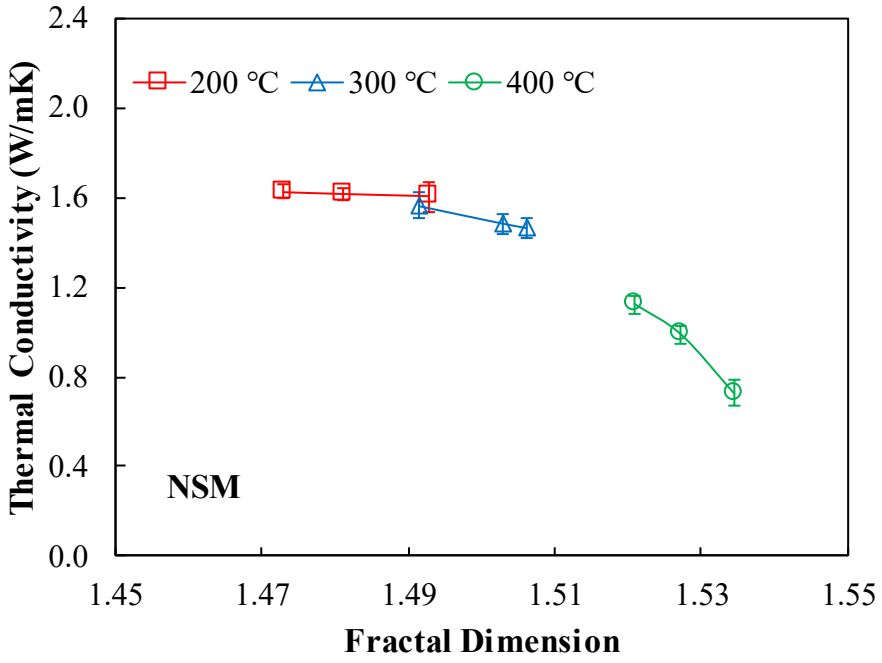

Figure 4.8 (a) Effect of fractal dimension on thermal conductivity of NSM

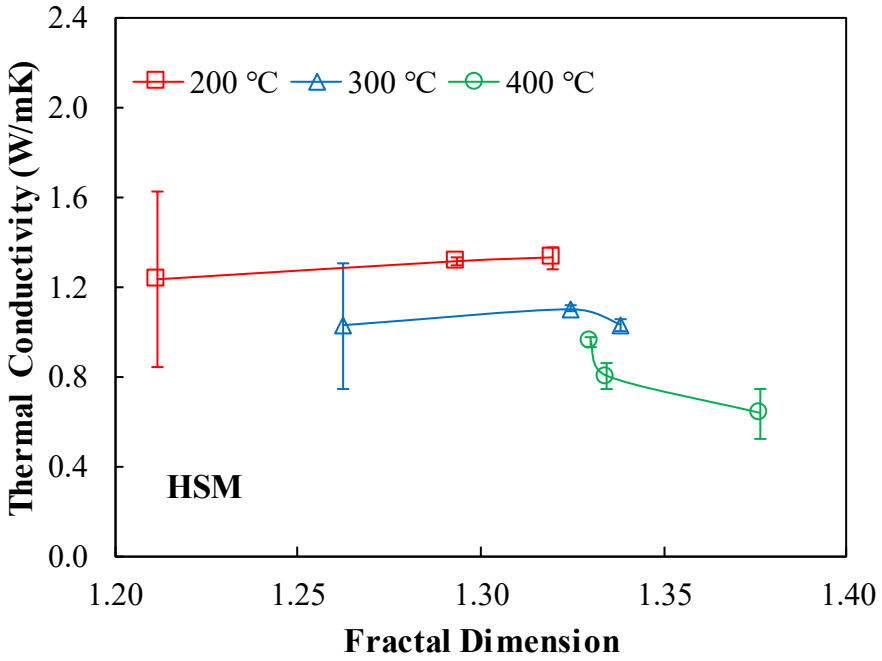

Figure 4.8 (b) Effect of fractal dimension on thermal conductivity of HSM

In Figure 4.8, the effect of fractal dimension, FD, on thermal constants for both mixes is presented. For NSM, thermal conductivity monotonically decreases with an increase in the FD. Combining the results from both recorded weight loss and porosity, the effect of mass transfer

on NSM is not very significant. Additional micro-cracks provides sufficient barrier for heat transfer at high heating rate, therefore thermal conductivity simply decreases as fractal increases. The situation is changed when it comes to HSM. Although the total porosity of HSM is much lower than NSM, Figure 4.6(b) from previous section indicates dramatically increase in weight loss when specimen is heated at the lowest rate. The effect of dehydration together with change in porosity cause an increase in the thermal conductivity at 200°C. Thereafter, micro-cracks play a dominate role as target temperature rises above 300°C. As a result, the thermal conductivity drops for an increase in FD.

4.4.2. Specific Heat

The specific heat capacities of mortar specimens are plotted in Figure 4.9 (a) for NSM and 4.9 (b) for HSM. A similar behavior was reported in Dos Santos. W. (2003), whereby the specific heat reaches a small peak between 200°C and 300°C, then decrease to a minimum value around 400°C, and gradually increases afterwards. It is likely that the influence of moisture on specific heat is relatively significant since the total weight loss is much higher. The specific heat of water is 4 to 5 times higher than ordinary concrete. As mentioned before, the peak evaporation of bonded water occurs around 270°C. At this temperature, the input of heat is mostly supplied to water removal but only a small amount of energy is used to raise the temperature of specimen (Kodur 2003c). Therefore an increase in specific heat is observed at 300°C.Since the specific heat of mortar is mostly dependent on the presence of water at lower temperatures, the effect of weight loss shows more significance at this point. The weight loss for NSM as seen in Figure 4.6(a) exhibit negligible differences between all three heating rates under 300°C. Therefore the specific heat is also less rate dependent up to 300°C. In the case of HSM, the weight loss at three heating rates are observed more dispersed from each other in Figure 4.6(b), showing more heating rate dependence. As the result, Figure 4.9 (b) displays conspicuous relationships of specific heat and heating rate at all temperatures. Note that the increase in specific heat at 300°C shows an opposite relationship of heating time and with presence of moisture.

At 400°C, the curve shows a drastic drop in specific heat over heating rate. This phenomenon

can be explained in the same way as the behaviour of thermal conductivity discussed above. Although specific heat is highly dependent on the presence of moisture, most of the water molecules chemically bounded in C-S-H have been evaporated at 400°C (Al-Sibahy and Edwards 2012). The specific heat at this temperature can be mostly attribute to the presence of quartz from silica sand. The specific heat of SiO_2 material like quartz exhibits positive linear temperature dependence (Zellar 1971). It simply increases at temperature rises. At high heating rate, the presence of temperature gradient and pore pressure cause large cracking through sand grains. This inconsistency of crystalline structure can be the reason for this dramatic drop in specific heat.

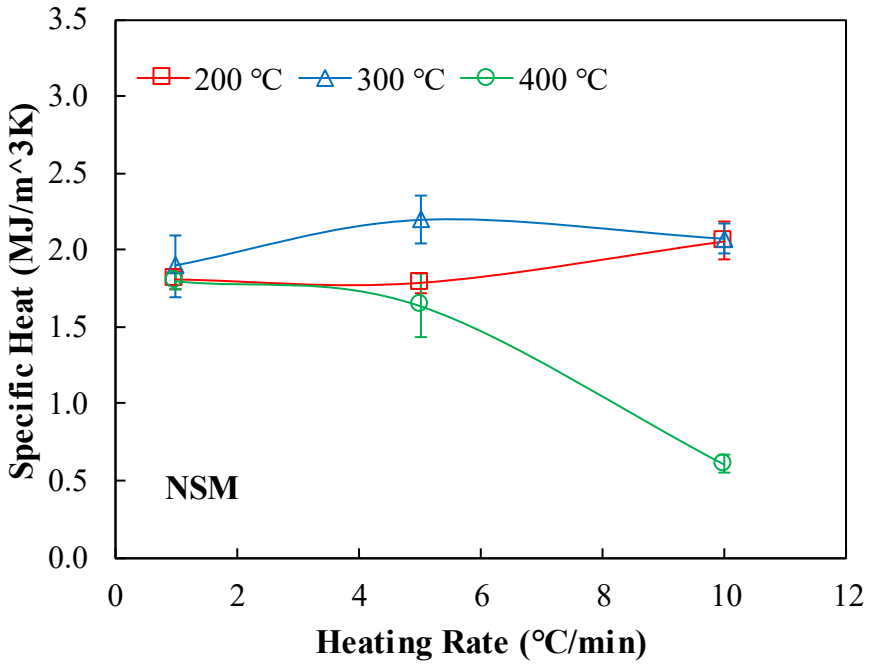

Figure 4.9(a) Effect of heating rate on specific heat of NSM at elevated target temperatures

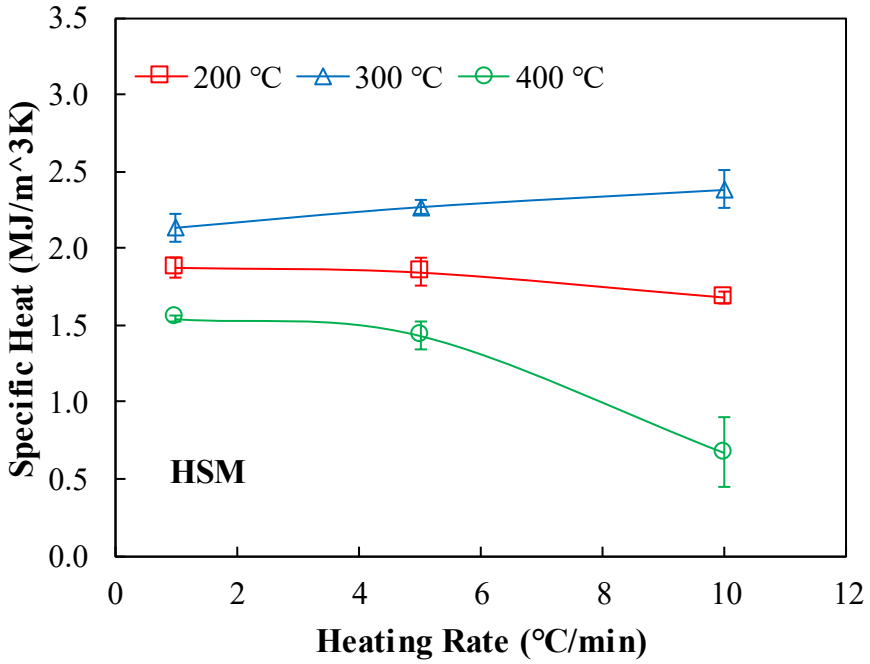

Figure 4.9(b) Effect of heating rate on specific heat of HSM at elevated target temperatures

The specific heat capacities of NSM and HSM are plotted against the fractal dimension, FD, in Figure 4.5 (a) and (b) respectively. The specific heat of hydrated cement materials is highly dependent on the presence of moisture. The physical damage of mortar specimens during heating impacts their specific heat only at 400°C. Therefore, the plots of specific heat over FD show less fractal dependence as expected.

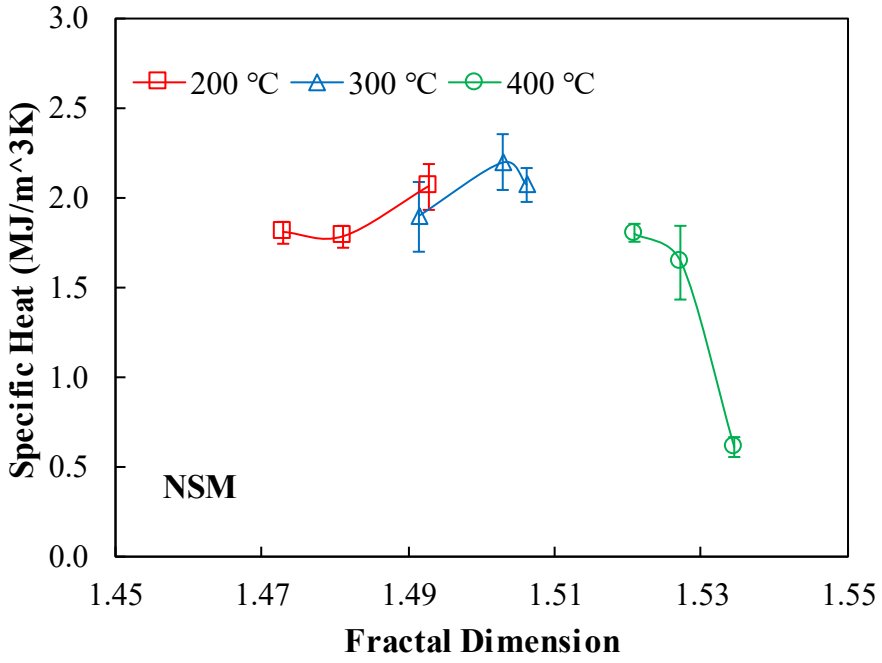

Figure 4.10 (a) Effect of fractal dimension on specific heat of NSM

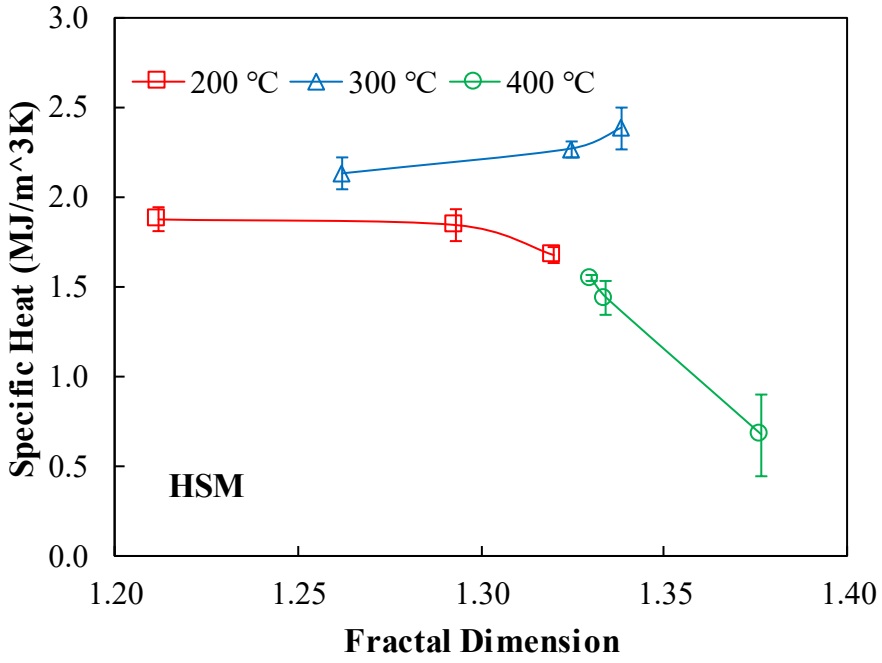

Figure 4.10 (b) Effect of fractal dimension on specific heat of HSM

3.5 Conclusion

Based on the data evaluated in this paper, the following conclusions may be drawn:

- The observed weight loss in HSM is dramatically higher than NSM across all heating rates
- Aside from thermal conductivity alone, the final temperature also gives influence on the relationship between thermal conductivity and heating rate;
- The total weight loss and associated variation of porosity level does limited effect on the behaviour of thermal conductivity for NSM;
- The thermal conductivity of NSM decreases as heating rate increases with high final temperatures due to additional thermally induced micro-cracks and contribution of quartz
- The thermal conductivity of HSM increases as heating rate increases at low temperature due to higher level of total weight loss. With high final temperatures, the thermal conductivity returns to decreased trend as heating rate increases;
- The specific heat is less heating rate dependent with low final temperatures for NSM
- The specific heat increases as heating rate decrease with high final temperatures can be caused by large cracks through sand grains
- The thermal conductivity monotonically decreases as FD increases for NSM, but HSM only shows similar trend at high targeting temperature;
- The specific heat show less fractal dependence as expected since it is mostly related to the presence of moisture and bound water inside mortar specimens.

Chapter 5 Conclusions

5.1 Concluding Remarks

Spalling is the biggest challenge in the use of concrete exposed to elevated temperatures. Studies have shown the combined effect of thermal and pore pressures is one of the main factors triggering the spalling phenomenon. Since thermal gradient inside concrete can potentially control the spalling phenomenon, it is necessary to conduct experimental investigations on the effect of heating rate on the thermal properties. Although prior studies have already taken the two parameters into account, spalling of concrete cannot yet be completely explained due to the lack of connections between thermal properties and heating rate. Moreover, the effect of heating rate on features of concrete micro-structure has not been fully investigated. Therefore, the main goal of this research project is to investigate the influence of heating rate on thermal properties and micro-structure of cement mortar. Given that high strength concrete has a more densified microstructure, the associated hindrance to water and steam transport increases the chances for spalling. In this study, a normal strength mortar designed to achieve 20 MPa, was compared with a high strength mortar designed to achieve 80 MPa, both at 7 days.

Based on the findings presented in this thesis, the following conclusions are drawn:

- The microstructure of high strength mortar (HSM) sample is more sensitive to heating rate compared to that of the normal strength mortar (NSM) sample in this study. Although the variation of heating rate has limited effect on the critical pore radius, it appears to be more pronounced in case of pore size distribution, and especially at higher sustained temperatures;
- The pore fraction as obtained from image analysis, decreased with an increase in the heating rate, across all temperatures of exposure. It appears that the slope of the curves drops with an increase in the heating rate, which indicates a reduction in heating rate sensitivity beyond a certain rate;

- The fractal dimension of the porous phase increases with an increase in the heating rate for both NSM and HSM specimens. As well, this fractal dimension increases with an increase in the temperature of exposure. The influence of pore coarsening on fractal dimension, caused by thermal decomposition of hydration products, was visible across all heating regimes;
- The thermal investigations of this work reveal that the thermal conductivity of NSM drops for an increase in the heating rate, up to a target temperature of 400°C. The drop in thermal conductivity may be attributed to the increase in the number of thermally induced micro-cracks. Even at lower rates of heating, the larger proportion of quartz in NSM led to higher thermal conductivity;
- The total weight loss and associated variation in porosity shows a positive correlation with temperatures of exposure. Moreover, the observed weight loss in HSM is dramatically higher than that in NSM, across all heating rates. It is evident from these trends that the porosity in both NSM and HSM increases as a consequence of thermal decomposition of hydrated cement paste as well as the formation of micro-cracks;
- Beyond an exposure temperature of 300°C, the specific heat of HSM decreases with an increase in the heating rate which may be attributed to the large cracks caused by thermal degradations.
- A correlation has been established between thermal constants and the pore fractal dimension in mortar. The thermal conductivity monotonically decreases with fractal dimension. While equally true for HSM, it was significant only at the highest temperature examined here.

5.2 Application of the Findings

Explosive spalling of high strength concrete is one of the most severe performance related phenomena. In modern concrete construction, HSC has been widely applied to high-rise buildings and tunnels. The failure of HSC under extreme temperatures compromises the intended function of the structure. Studies have shown that the heating rate is one of the main factors associated with spalling. Therefore, an investigation connecting heating rate with

thermal properties and micro-structural features will help to predict the behavior of the structural member during extreme thermal exposure. To this end, the findings of this study on quantifying the air-void network and thermal characterization for mortar as they evolve at different heating rates are expected to help design durable mixtures, with better resistance to spalling. The experimental outcomes can specifically help as follows:

- The concept of fractal dimension and its correlation with heating rate are potentially beneficial in simulating the behavior of a concrete member during heat exposure;
- Experimentally investigated results on thermal conductivity and specific heat can be used to simulate heat and mass transfer at different heating rates. These in turn may be utilized in predicting explosive spalling.

5.3 Prospects for future works

This thesis makes an effort towards reducing the knowledge gap described in Chapters 1 & 2, to correlate the thermal properties under various heating rates with the evolution of microstructure. Prospects for further studies are as follows:

- Tortuosity of mortar needs to be studied under different heating conditions;
- In this work, only one type of method is conducted to obtain each experimental results. A generally accepted method should be proposed based on the comparison of various methods;
- Although the mortar mixtures incorporated a polymeric (PET) fibre, this study did not examine the role of fibres on the changes to the microstructure or thermal constants. Further studies should investigate the benefits from fibres at varying heating rates on these parameters.;
- Effect of heating rate on mortar beyond 400°C should be studied. Further investigation is recommended to explore the effect of heating rate by taking different scenarios of hygric equilibrium into account.

References

ASTM C33, A. (2004) Standard specification for concrete aggregates. American Society for Testing and Material, 1-11

ASTM C39/C39M-12 (2012). Standard test method for compressive strength of cylindrical concrete specimens.

ASTM C150/C150M-18 (2018) Standard Specification for Portland Cement, ASTM International, West Conshohocken, PA

ASTM C192/C192M-16a (2016) Standard Practice for Making and Curing Concrete Test Specimens in the Laboratory, ASTM International, West Conshohocken, PA

ASTM C617/C617M-15 (2015) Standard Practice for Capping Cylindrical Concrete Specimens, ASTM International, West Conshohocken, PA

ASTM C618-17a (2017) Standard Specification for Coal Fly Ash and Raw or Calcined Natural Pozzolan for Use in Concrete, ASTM International, West Conshohocken, PA

ASTM C1437 (2001) Standard test method for flow of hydraulic cement mortar. Philadelphia, PA.

ASTM D695-15 (2015) Standard Test Method for Compressive Properties of Rigid Plastics, ASTM International, West Conshohocken, PA

ASTM D7984-16 (2016) Standard Test Method for Measurement of Thermal Effusivity of Fabrics Using a Modified Transient Plane Source (MTPS) Instrument. ASTM International, West Conshohocken, PA

ASTM STP 169D. (2006). Significance of tests and properties of concrete and concrete-making materials. ASTM International, 246-247.

Al-Sibahy and Edwards (2012) “Thermal behaviour of novel lightweight concrete at ambient and elevated temperatures: Experimental, modelling and parametric studies” Construction and Building Materials 31 (2012) 174–187.

Ali F. A et al (2001) “Explosive spalling of high-strength concrete columns in fire” Magazine of Concrete Research, 2001, 53, No. 3, June, 197–204.

Bazant, Z. P. (1997). “Analysis of pore pressure, thermal stress and fracture in rapidly heated concrete.” 155–164.

Berman R. (1976) “Thermal conduction in solids” Chap 9, p. 104-110, Clarendon press, Oxford

Bilodeau A, Kodur V.K. R, Hoff GC. (2004) “Optimization of the type and amount of polypropylene fibres for preventing the spalling of lightweight concrete subjected to hydrocarbon fire” Cem Concr Compos J 2004; 26(2): 163–75.

Bouguerra, A., Aït-Mokhtar, A., Amiri, O. & Diop, M. B. (2001) “Measurement of thermal conductivity, thermal diffusivity and heat capacity of highly porous building materials using transient plane source” technique. Int. Commun. Heat Mass Transf. 28, 1065–1078.

Chan S. Y. N., Luo X. and Sun W. (2000a) “Effect of high temperature and cooling regimes on the compressive strength and pore properties of high performance concrete” Construction and Building Materials, Volume 14, Issue 5, Pages 261-266, ISSN 0950-0618.

Chan, Y. N., Luo, X., and Sun, W. (2000b). “Compressive strength and pore structure of high-performance concrete after exposure to high temperature up to 800 C.” Cement and Concrete Research, 30(2), 247–251.

Chan Y. N., Peng G. F., Anson M. (1999) “Residual strength and pore structure of high-strength concrete and normal strength concrete after exposure to high temperatures” Cement and Concrete Composites, Volume 21, Issue 1, Pages 23-27, ISSN 0958-9465.

Charlaix E., Guyon E. and Roux S. (1987) “Permeability of a random array offractures of widely varying apertures” Transp. Porous Media 2, 31–43.

Colin T. Davie , Chris J. Pearce & Nenad Bićanić (2006) “Coupled Heat andMoisture Transport in Concrete at Elevated Temperatures—Effects of Capillary Pressure and Adsorbed Water”, Numerical Heat Transfer, Part A: Applications, 49:8, 733-763.

Comeau, E.; Wolf, A. (1997). "Fire in the Chunnel" NFPA Journal.

Copier W. J. (1979) “Spalling of normal weight and lightweight concrete on exposure to fire.” Report 24(2), Heron, Holland.

Canadian Standards Association. (2013). CSA A3000-13 Cementitious Materials Compendium. CSA Group, Mississauga, Ontario.

Della M. R. (1988) “Relationships between Permeability, Porosity, Diffusion and Microstructure of Cement Pastes, Mortar, and Concrete at Different Temperatures” Materials Research Laboratory, The Pennsylvania State University, Park, Pennsylvania 16802.

Diamond, S. (1999). “Aspects of concrete porosity revisited.” Cement and Concrete Research, 29(8), 1181–1188.

Diamond, S. (2000). “Mercury porosimetry: An inappropriate method for the measurement of pore size distributions in cement-based materials.” Cement and Concrete Research, 30(10), 1517–1525.

Diamond S. and Huang J. (2001) “The ITZ in concrete – a different view based on image analysis and SEM observations” Cement and Concrete Composites, Volume 23, Issues 2–3, Pages 179-188, ISSN 0958-9465.

dos Santos. W. (2001) “Effect of moisture and porosity on the thermal properties of a conventional refractory concrete” Journal of the European Ceramic Society 23 (2003) 745–755

Fernando P., Oscar R. K. M., Philippe J. P. G. and Humberto R. R. (2012) “Mechanical Properties of Recycled PET Fibers in Concrete” Materials Research. 2012; 15(4): 679-686.

Fu Y. and Li L. (2011) “Study on mechanism of thermal spalling in concrete exposed to elevated temperatures” Materials and Structures (2011) 44:361–376.

Formosa J, Chimenos JM, Lacasta AM, Haurie L, Rosell JR. (2011) “Novel fire-protecting mortars formulated with magnesium by-products” Cem Concr Res ;41:191–6.

Gawin D., Majorana C. E. and Schreßer B. A. (1999) “Numerical analysis of hygro-thermal behaviour and damage of concrete at high temperature” Mechanics of Cohesive-frictional Materials, 4, 37Ð74.

Grandet J., Ollivier J. P. (1975) “New Method for the study of cement-aggregate interfaces.” Proceedings of the Seventh Intemational Congress Chem Cement, Paris Vol. III. p. VII 85-VII 9.

Goncalves JRA, Boluk Y and Bindiganavile V (2018) “Thermal properties of fibre-reinforced alkali-activated concrete in extreme temperatures” Magazine of Concrete Research 70(18): 954–964

Hager, I. (2013) “Behaviour of cement concrete at high temperature” Bulletin of the Polish Academy of Sciences Technical Sciences, Vol. 61, No. 1, 2013.

Hu L, Liu S, Xu Y. (2011) “A wind tunnel experimental study on burning rate enhancement behaviour of gasoline pool fires by cross air flow” Combustion and Flame 158 (2011) 586–591.

Kearsley E. P., Wainwright P. J (2001) “Porosity and permeability of foamed concrete” Cement and Concrete Research 31 805-812

Khan M. I. (2011) “Factors a!ecting the thermal properties of concrete and applicability of its prediction models” Building and Environment 37 (2002) 607–614.

Kim K. H., Jeon, S. E. (2003) “An experimental study on thermal conductivity of concrete” Cement and Concrete Research 33 (2003) 363–371

Kirkland, C. J. (2002). "The fire in the Channel Tunnel" (PDF). Tunnelling and Underground Space Technology. 17 (2): 129–132.

Kodur V. K. R. and Khaliq W. (2010) “Effect of Temperature on Thermal Properties of Different Types of High-Strength Concrete” Journal of Materials in Civil Engineering, Vol 23, Issue 6

Kodur V. K. R., Khaliq W and Raut N. (2013) “An approach to account for tie configuration in predicting fire resistance of reinforced concrete columns” Engineering Structures 56 (2013) 1976–1985.

Kodur V. K. R., Phan L. (2007) “Critical factors governing the fire performance of high strength concrete systems” Fire Safety Journal 42 (2007) 482–488.

Kodur V. K. R, Sultan M. A. (1998) “Structural behavior of high strength concrete columns exposed to fire. In: Proceedings: international symposium on high performance and reactive powder concrete” vol.4, Sherbrooke, Quebec; 1998. p. 217–32.

Kodur V. K. R, Cheng F. P, Wang T. C. (2003a) “Effect of strength and fiber reinforcement on the fire resistance of high strength concrete columns.” ASCE J Struct Eng 2003;129 (2):253–9.

Kodur V. K. R, McGrath RC. (2003b)“Fire endurance of high strength concrete columns. Fire Technology—Special Issue 2003; 39(1): 73–87.

Kodur V. K. R and Sultan M. A. (2003c) “Effect of Temperature on Thermal Properties of High-Strength Concrete” Journal of Materials in Civil Engineering Vol. 15, Issue 2.

Kodur V. K. R, Wang T. C, Cheng F. P. (2004a)“Predicting the fire resistance behaviour of high strength concrete columns” Cem Concr Compos J 2004; 26: 141–53.

Kodur V. K. R (2004b) “Properties of Concrete at Elevated Temperatures” Hindawi Publishing Corporation, ISRN Civil Engineering.

Kodur V. K. R, McGrath R. (2006) “Effect of silica fume and lateral confinement on fire endurance of high strength concrete columns” Can J Civ Eng 2006;33:93–102.

Khaliq W. and Kodur V. K. R. (2011) “Thermal and mechanical properties of fiber reinforced high performance self-consolidating concrete at elevated temperatures” Cement and Concrete Research 41 (2011) 1112–1122

Khoury G. (2005) “Spalling Review- Types, Assessment and Prevention, UPTUN report WP 4” Project GRD1-2001-40739, 5th Framework Program of the European Union Competitive and Sustainable Growth.

Le Q. X., Dao, V. TN (2018) “Effects of temperature and temperature gradient on concrete performance at elevated temperatures” Advances in Structural Engineering 2018, Vol. 21(8) 1223–1233

Liu F (2015) “On the Prediction of Concrete Spalling Under Fire” PhD thesis, ETH Zurich Research Collection.

Liu W.V. et al (2014) “Thermal properties of lightweight dry-mix shotcrete containing.

Expanded perlite aggregate” Cement & Concrete Composites 53 (2014) 44–51

Luo, X., Sun, W. and Chan, S. Y. N. (2000) “Effect of heating and cooling regimes on residual strength and microstructure of normal strength and high-performance concrete” Cement and Concrete Research 30 379-383.

Luo, X., Sun, W. and Chan, S. Y. N. (2000) “Residual compressive strength and microstructure of high performance concrete after exposure to high temperature” at. Struct. (2000) 33: 294.

Mandelbrot B.B. (1982) “The Fractal Geometry of Nature”, Freeman Publishers, New York, 1982.

Meyer-Ottens, C. (1972) “The question of spalling of concrete structural elements of standard concrete under fire loading.” PhD Thesis, Technical University of Braunschweig, Germany.

Mindeguia, J. C., Pimienta, P., Noumowé, A., & Kanema, M. (2010). Temperature, pore pressure and mass variation of concrete subjected to high temperature—experimental and numerical discussion on spalling risk. Cement and Concrete Research, 40(3), 477-487.

Noumowe A. (2005) “Mechanical properties and microstructure of high strength concrete containing polypropylene fibres exposed to temperatures up to 200-C” Cement and Concrete Research 35 (2005) 2192–2198.

Ollivier J.P., Maso J.C., Bourdette B. (1995) “Interfacial transition zone in concrete” Advanced Cement Based Materials, Volume 2, Issue 1, Pages 30-38, ISSN 1065-7355.

Phan, L. T., Lawson, j. R. and Davis F. L. (2001) “Effects of elevated temperature exposure on heating characteristics, spailing, and residual properties of high performance concrete” Materials and Structures/Mat6riaux et Constructions, Vol. 34, March 2001, pp 83-91.

Pierre K., Grégoire C. and Christophe G. (2001) “High-temperature behaviour of HSC with polypropylene fibres: From spalling to microstructure” Cement and Concrete Research, Volume 31, Issue 10, Pages 1487-1499, ISSN 0008-8846.

Richardson L.F. (1961) “The Problem of Contiguity: An Appendix of Statis-tics of Deadly Quarrels”, General Systems Yearbook, Vol. 6, 1961, pp.139–187.

Rostasy F. S., Weib R., and Wiedemann G. (1980) “Change of Pore Structure of Cement Mortars due to Temperature” Cement and Concrete Research. Vol. I0, pp. 157-164.

Russ J.C. (1992) “Fractal Surfaces”, Plenum Press, New York, 1992.

Saad M., Abo-El-Eneint S. A., Hnna G. B and Kotkata M. F. (1996) “Effect of temperature on physical and mechanical properties of concrete containing silica fume” Cement and Concrete Research, Vol. 26, No 5, pp 669-675

Sancak E., Saro D. Y., Simek O. (2008) “Effects of elevated temperature on compressive strength and weight loss of the light-weight concrete with silica fume and superplasticizer” Cement and Concrete Composites 30 715-721

Scrivener, K. L. (1989). “The Use of Backscattered Electron Microscopy and Image Analysis to Study the Porosity of Cement Paste.” Proceedings of Symposium on Pore Structure and Permeability of Cementitious Materials, MRS Online Proceedings Library Archive, 129–140.

Scrivener, K. L. (2004). “Backscattered electron imaging of cementitious microstructures: understanding and quantification” Cement & Concrete Composites 26 935-945

Silva D. A., Betioli A. M., Gleize P. J. P., Roman H. R., Go´mez L.A. and Ribeiro J. L. D. (2005) “Degradation of recycled PET fibers in Portland cement-based materials” Cement and Concrete Research 35 (2005) 1741–1746.

Saouma V. E. (1994) “Fractals, Fractures, and Size Effects in Concrete” Journal of Engineering Mechanics, Vol 120 Issue 4.

Snydewr K. A., Bentz D. P. Garboczi E. J and Winslow D. N (1992) “Interfacial zone percolation in cement-aggregate composites” In: Maso JC, editor. Interfaces in cementitious composites. RILEM Proceeding 18. E and FN Spon; p. 259-68.

Shoaib, M. M., Ahmed, S. A., Balaha, M. M. (2001). “Effect of fire and cooling mode on the properties of slag mortars” Cement and Concrete Research 31 (2001) 1533 – 1538.

Theiler J. (1990) "Estimating fractal dimension," J. Opt. Soc. Am. A 7, 1055-1073.

Tran H. C. and White H. R. (1992) “Burning Rate of Solid Wood Measured in a Heat Release Rate Calorimeter” FIRE AND MATERIALS, VOL. 16, 197-206 (1992)

Tsimbrovska, M., Kalifa, P., Quenard, D., and Daian, J. F. (1997) “High performance concretes at elevated temperature: permeability and microstructure.” Lyon, France, 475–482.

Vodák F., Trtík K., Kapičková O., Hošková Š. And Demo P. (2004) “The effect of temperature on strength – porosity relationship for concrete” Construction and Building Materials 18 (2004) 529–534.

Wang, Y., & Diamond, S. (1994) An Approach to Quantitative Image Analysis for Cement Pastes. MRS Proceedings, 370, 23. doi:10.1557/PROC-370-23.

Wang Y (1995), “Microstructural study of hardened cement paste by back-scatter scanning electron microscopy and image analysis”, Ph. D. the-sis, Purdue University, 1995.

Winslow, D. N. (1985). “The fractal nature of the surface of cement paste.” Cement and Concrete Research, 15(5), 817–824.

Wong, H. S., Head, M. K., and Buenfeld, N. R. (2006). “Pore segmentation of cement-based materials from backscattered electron images.” Cement and Concrete Research, 36(6), 1083–1090.

Xu. Y., Wong Y. L., Poon C. S. and Anson M. (2001) “Impact of high temperature on PFA concrete” Cement and Concrete Research 31 (2001) 1065–1073

Yang J. (2004) “Thermal conductivity: theory, properties, and applications” Theory of Thermal Conductivity, 2-3

Ye G., Liu X., Schutter De G., Taerwe L. and Vandevelde P. (2007) “Phase distribution and microstructural changes of self-compacting cement paste at elevated temperature” Cement and Concrete Research 37 (2007) 978–987.

Yu, B., and Li, J. (2001). “Some fractal characters of porous media.” Fractals, 09(03), 365–372.

Zhang B., Bicanic N. Pearce C. J. and Balabanic G. (2000) “Residual fracture properties of normal- and high-strength concrete subject to elevated temperatures” Magazine of Concrete Research 2000, 52, No. 2, 123-136.

Zhang B. (2011) “Effects of moisture evaporation (weight loss) on fracture properties of high performance concrete subjected to high temperatures” Fire Safety Journal 46 (2011) 543–549.

Zhao D., Qian X., Gu X., Jajja S. A. and Yang R. (2016) “Measurement Techniques for Thermal Conductivity and Interfacial Thermal Conductance of Bulk and Thin Film Materials” ASME. J. Electron. Packag. 2016;138(4):040802-040802-19. doi:10.1115/1.4034605.

Zeller R. C. and Pohl R. O. (1971) “Thermal Conductivity and Specific Heat of Noncrystalline Solids” Vol. 4, Iss. 6

Zhou Q. and Glasser F. P. (2001) “Thermal stability and decomposition mechanisms of ettringite at <120°C” Cement and Concrete Research 31 (2001) 1333 –1339.